Materials Research Letters

ISSN: (Print) 2166-3831 (Online) Journal homepage: http://www.tandfonline.com/loi/tmrl20

Fundamentals of Superior Properties in Bulk NanoSPD Materials

R.Z. Valiev, Y. Estrin, Z. Horita, T.G. Langdon, M.J. Zehetbauer & Y.T. Zhu

To cite this article: R.Z. Valiev, Y. Estrin, Z. Horita, T.G. Langdon, M.J. Zehetbauer & Y.T. Zhu (2016) Fundamentals of Superior Properties in Bulk NanoSPD Materials, Materials Research Letters, 4:1, 1-21, DOI: 10.1080/21663831.2015.1060543

To link to this article: http://dx.doi.org/10.1080/21663831.2015.1060543

© 2015 The Author(s). Published by Taylor & Francis.

Published online: 28 Jul 2015.

Submit your article to this journal

Article views: 1128

View related articles

View Crossmark data

Citing articles: 2 View citing articles

Full Terms & Conditions of access and use can be found at
http://www.tandfonline.com/action/journalInformation?journalCode=tmrl20

Download by: [University of Southampton] **Date:** 17 February 2016, At: 06:30

MATERIALS RESEARCH LETTERS

Mater. Res. Lett., 2016
Vol. 4, No. 1, 1–21, http://dx.doi.org/10.1080/21663831.2015.1060543

Taylor & Francis
Taylor & Francis Group

www.tandfonline.com/toc/tmrl20/current

Downloaded by [University of Southampton] at 06:30 17 February 2016

Fundamentals of Superior Properties in Bulk NanoSPD Materials

R.Z. Valiev[a,b*], Y. Estrin[c,d], Z. Horita[e,f], T.G. Langdon[g,h], M.J. Zehetbauer[i] and Y.T. Zhu[j,k]

[a]*Institute of Physics of Advanced Materials, Ufa State Aviation Technical University, Ufa 450000, Russia;* [b]*Laboratory for Mechanics of Bulk Nanomaterials, Saint Petersburg State University, Saint Petersburg 198504, Russia;* [c]*Centre for Advanced Hybrid Materials, Department of Materials Engineering, Monash University, Clayton, VIC 3800, Australia;* [d]*Laboratory of Hybrid Nanostructured Materials, Moscow Institute of Steel and Alloys, Moscow 119049, Russia;* [e]*Department of Materials Science and Engineering, Faculty of Engineering, Kyushu University, Fukuoka 819-0395, Japan;* [f] *WPI, International Institute for Carbon-Neutral Energy Research (WPI-I2CNER), Kyushu University, Fukuoka 819-0395, Japan;* [g]*Departments of Aerospace & Mechanical Engineering and Materials Science, University of Southern California, Los Angeles, CA 90089-1453, USA;* [h]*Materials Research Group, Faculty of Engineering and the Environment, University of Southampton, Southampton SO17 1BJ, UK;* [i]*Research Group Physics of Nanostructured Materials; Faculty of Physics, University of Vienna, Wien A-1090, Austria;* [j] *School of Materials Science and Engineering, Nanjing University of Science and Technology, Nanjing 210094, People's Republic of China;* [k]*Department of Materials Science and Engineering, North Carolina State University, Raleigh, NC 27695, USA*

(*Received 15 April 2015; final form 6 June 2015*)

Bulk nanoSPD materials are materials with nanostructural features, such as nanograins, nanoclusters, or nanotwins, produced by severe plastic deformation (SPD) techniques. Such nanostructured materials are fully dense and contamination free and in many cases they have superior mechanical and functional properties. Here, we provide a critical overview of such materials, with a focus on the fundamentals for the observed extraordinary properties. We discuss the unique nanostructures that lead to the superior properties, the underlying deformation mechanisms, the critical issues that remain to be investigated, future research directions, and the application potential of such materials.

Keywords: Severe Plastic Deformation, Ultrafine-grained Materials, Nanostructures, Properties

1. Introduction In recent years there has been growing interest in bulk nanostructured materials produced by severe plastic deformation (SPD) processing, as demonstrated by the increasing number of publications with high citations [1] as well as numerous specialized conferences, workshops and symposia on the subject (www.nanospd.org).

The critical feature of SPD, in which heavy straining is applied under high pressure with accumulated strains ε in excess of $\sim$4–6, makes it possible to produce ultrafine grains (UFG) with sizes smaller than 1,000 nm.[2–5] Processing by SPD may also lead to a dissolution of second phases, precipitation, amorphization, and other processes producing various nanostructural features such as deformation twins, non-equilibrium grain boundaries, dislocation substructures, solute segregation,[6] and clusters. These changes in the inner make-up of the material may affect the deformation mechanisms and, consequently, change the material properties in a fundamental way. As a result, new structural and functional metals and alloys having superior and unique properties have been developed by SPD processing. [4,7–10]

Over the last decade there has been extensive research into the mechanical and functional properties of bulk nanostructured materials as well as their origin and relationship to fundamental physics. This report gives a critical overview of this research with special attention directed to the extraordinary properties that are enabled by SPD. Our views on the prospects for future developments in the area of nanoSPD materials are also outlined.

*Corresponding author. Email: rzvaliev@mail.rb.ru

© 2015 The Author(s). Published by Taylor & Francis.
This is an Open Access article distributed under the terms of the Creative Commons Attribution License (http://creativecommons.org/licenses/by/4.0/), which permits unrestricted use, distribution, and reproduction in any medium, provided the original work is properly cited.

Downloaded by [University of Southampton] at 06:30 17 February 2016

2. Grain Boundaries and Other Crystal Lattice Defects Generated by SPD Grain boundaries in nanostructured materials affect their properties in very significant ways and quite often the UFG metals are referred to as 'interface-controlled materials'. Different types of grain boundaries are formed by SPD processing and they may be classified as [2,7]

- Low- vs. high-angle boundaries;
- Special vs. random boundaries;
- Equilibrium vs. non-equilibrium boundaries with strain-distorted structures.

In addition, SPD may also produce other structural features in alloys, such as second-phase particles, nanotwins, and solid segregations at the grain boundaries. Such modifications of the make-up of the material at the nano scale can have a strong effect on the material properties. The use of advanced imaging and structural characterization techniques over the past decade has brought about the discovery of three significant nanostructural features of SPD-processed alloys,[8,10–16] which give rise to their remarkable mechanical and functional properties. These are outlined below.

2.1. Nanotwins. A high density of nanotwins produced by SPD was found to increase both the strength and ductility of nanostructured metals and alloys. Figure 1 shows a transmission electron microscopy (TEM) image of UFG Cu after equal-channel angular pressing (ECAP) and cryorolling at the liquid nitrogen temperature; twins 10–20 nm in width are clearly visible.[12] To promote the formation of nanotwins, the following intrinsic material properties and external deformation conditions are required [11]: (1) a relatively low stacking fault energy, (2) a low deformation temperature, and (3) a high strain rate. It should be noted that there is an optimum grain size range conducive for deformation twinning.[11,17–19] This optimum grain size for the formation of deformation twins is affected by both intrinsic properties of the material mentioned above, and it can be estimated using the following equation [11]:

$$\frac{d_{\mathrm{m}}}{\ln(\sqrt{2}d_{\mathrm{m}}/a)} = \frac{9.69 - \nu}{253.66(1-\nu)}\frac{Ga^2}{\gamma}, \qquad (1)$$

where γ is the stacking fault energy, a is the lattice parameter, ν is Poisson's ratio, G is the shear modulus, and d_{m} is the optimum grain size.

2.2. Clusters and Segregations. It was found by 3D atom probe tomography that SPD may hinder the formation of precipitates in age-hardenable alloys and instead promote clustering and segregation of alloying elements.[7,15,20–22] For example, the data in Figure 2 [23] show that segregations at grain boundaries make-up clusters ~3–5 nm wide in the age-hardenable Al alloy 7075. Moreover, the concentration of alloying elements may be an order of magnitude higher at grain boundaries than in the grain interior.[8,20,22,23]

2.3. Nanosized Particles and Secondary Phase Precipitations. In many alloys subjected to SPD after solid-solution hardening, high densities of nanosized particles appear.[8,10,24] Figure 3 shows an example of nanoparticles that are ~10–20 nm in size in the UFG Al alloy 6061 after ECAP.[24] The presence of

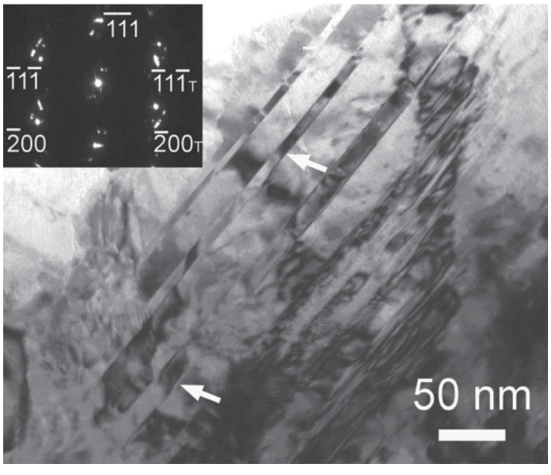

Figure 1. Typical bright-field TEM images of a grain with high density of deformation nanotwins in UFG Cu that was subjected to ECAP and subsequent cryogenic rolling.[12]

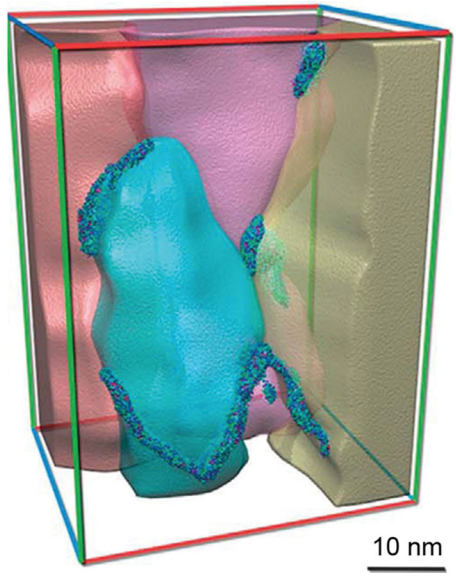

Figure 2. Tomographic image of nanostructure of UFG Al alloy 7075. Segregations of alloying elements on grain boundaries and at triple junctions are shown.[22]

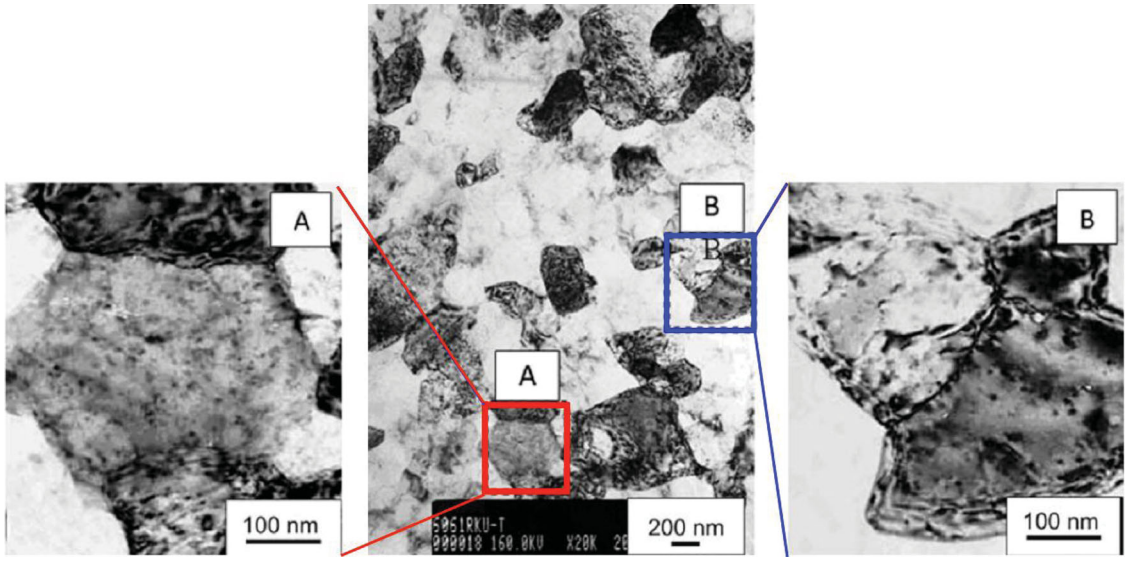

Figure 3. UFG structure of Al alloy 6061 after ECAP in parallel channels (four passes): nanosized precipitations in grains are clearly visible in areas A and B at higher magnification.[24]

Downloaded by [University of Southampton] at 06:30 17 February 2016

these nanoparticles is due to dynamic aging and the high density of nucleation sites generated by entangled dislocations. The small size and high density of such particles effectively block and accumulate dislocations not only causing higher strength but also promoting ductility.[13,23–25]

Thus, UFG metals and alloys produced by SPD methods are characterized by a number of nanostructural features which can strongly influence their behavior. In many demonstrated cases, the properties induced by SPD processing are unique to these materials, as will be shown in the following sections.

3. Mechanical Properties of Bulk Nanostructured Materials

Three major properties, namely strength, fatigue behavior and superplasticity, are considered in this section.

3.1. Superior Strength and Ductility.

A primary advantage of SPD processing is strength enhancement. Even though the well-known Hall–Petch relation between the yield stress σ_y and the grain size d,

$$\sigma_y = \sigma_0 + K_{\mathrm{HP}} d^{-1/2}, \tag{2}$$

may break down for nanomaterials, it commonly holds for UFG materials produced by SPD. Here, σ_0 and K_{HP} are constants for a given material. Typically, extreme grain refinement by SPD can improve the strength of pure metals or dilute alloys by a factor of 3–8.[26–30] For SPD-processed alloys, grain refinement is often accompanied by phase transformations leading to the formation of nanoclusters, segregations, nanotwins, and dislocation substructures, which provide additional hardening mechanisms. In particular, the formation of grain boundary segregations in the UFG alloys by SPD may suppress the generation of dislocations at grain boundaries and lead to considerable additional hardening.[23] For example, Figure 4 shows the tensile stress–strain curves of the Al alloys 1570 and 7475. It is seen that the alloys which acquired their UFG structure by high-pressure torsion (HPT) are more than twice as strong as those subjected to conventional hardening.

It was shown [23] that for bulk nanostructured alloys with a grain size of 100–130 nm, the magnitude of σ_y is considerably higher than the value calculated from the Hall–Petch relationship. This phenomenon of superstrength of nanostructured alloys was recently demonstrated in various SPD-processed materials, including Al alloys,[24,31] Ti alloys,[8] carbon steels and stainless steels,[32–34] and in an Al–Mg nanocomposite.[35] However, increasing strength of metals and alloys through grain refinement by SPD usually leads to an undesirable drop in their ductility.[8,10,36,37]

The low ductility is caused by the reduction of the strain-hardening capability of a severely deformed material. This can be rationalized in terms of the Considère criterion which states that failure by necking under tensile loading will not occur if the following inequality is fulfilled:

$$\left(\frac{d\sigma^{\mathrm{T}}}{d\varepsilon^{\mathrm{T}}}\right)_{\dot{\varepsilon}} \geq \sigma^{\mathrm{T}}, \tag{3}$$

where σ^{T} and ε^{T} denote the true stress and true strain, respectively. On the other hand, grain refinement enhances the strain rate sensitivity (SRS) of the flow stress and this helps preventing necking.[38] Therefore,

Downloaded by [University of Southampton] at 06:30 17 February 2016

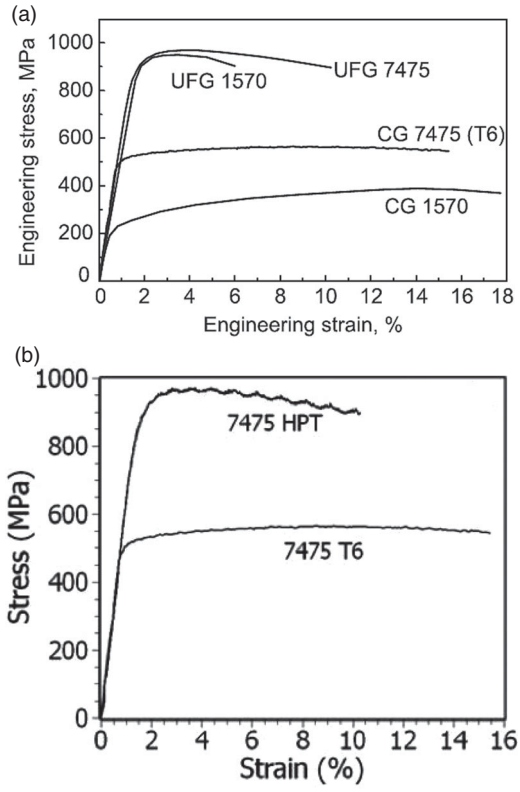

Figure 4. Engineering stress–strain curves of the UFG alloys Al 1570 (a) and Al 7475 (b) processed by HPT in comparison with standard treatment.[23]

these two factors compete with each other in affecting the tensile ductility.[39] The effect of the SRS increase is usually weaker than the effect of the strain-hardening reduction, which explains the low ductility of UFG materials except at relatively high homologous temperatures. Indeed, high ductility was reported in nanostructured zinc [40,41] which has a low melting point of 692.68 K.

There have been some exceptions where UFG and nanostructured metals exhibited both high strength and high ductility.[42–47] The primary reason for the low ductility of nanostructured and UFG metals and alloys is their low strain-hardening rate. In recent years, great efforts were made to design microstructures and deformation mechanisms that will increase the strain-hardening rate, some of which lead to an increase in both strength and ductility.[5,25] Reported successful strategies include inducing effects that promote the occurrence of a high density of twin boundaries,[12,48,49] lowering the stacking fault energy to activate deformation twinning,[12,14,50] introducing a high density of second-phase nanoparticles,[13,51] or through grain boundary engineering.[52,53] More recently, an alternative strategy that relies on gradient structures was shown to be very effective in improving ductility.[54–57]

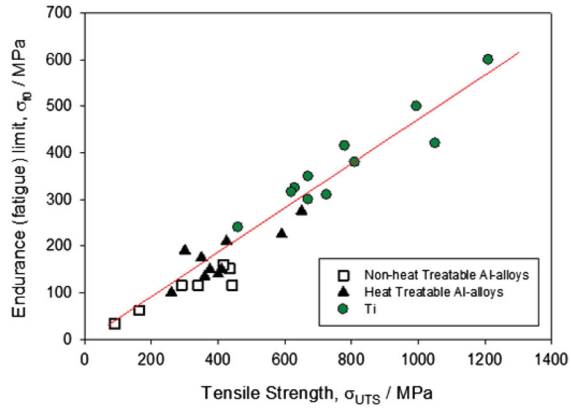

Figure 5. Empirical correlation between the fatigue limit and the UTS for UFG Ti and Al alloys.[59]

3.2. Fatigue Behavior. Fatigue resistance is important for many applications of UFG materials and there has been extensive research in this area. Recent literature surveys on fatigue properties of SPD-processed materials can be found elsewhere.[9,58,59] Empirically, the fatigue limit of coarse-grained materials is proportional to the ultimate tensile strength (UTS) (Figure 5) [59] which may be used to estimate the fatigue limit. However, the fatigue behavior of SPD-processed metals in general is determined by both strength and ductility. Specifically, high-cycle fatigue (HCF) is controlled by the resistance of the material to crack initiation, while low cycle fatigue (LCF) is governed by crack propagation. The life under LCF is largely controlled by ductility while that under HCF is dictated by the fracture strength. Consequently, when SPD processing raises the tensile strength at the cost of ductility, the HCF life is improved while the LCF life is decreased. Again, there are fortunate exceptions to this disadvantageous juncture. It was found [60,61] that ECAP of dilute Cu–Cr–Zr alloys followed by an aging treatment leads to a remarkable improvement of tensile strength and fatigue strength in the HCF regime without sacrificing ductility and LCF properties. Similarly, extrusion + ECAP processing of the ZK60 Mg alloy was shown to lead to an excellent combination of strength and ductility [62] and also brought an impressive improvement of fatigue properties over the entire range of stress amplitudes tested (see Figure 6).[63]

SPD processing also produces good fatigue performance in other metals and alloys. For example, it was reported [64] that an ECAP-processed stainless steel had a record-high fatigue limit due to profuse deformation twinning induced by severe straining. Another example is SPD-processed commercial purity titanium that showed record values of fatigue strength (which were close to or in excess of those for the conventional alloy Ti-6Al-4V).[65–67] These results make it promising to replace this potentially toxic alloy with pure Ti in biomedical applications (see Section 4.8).

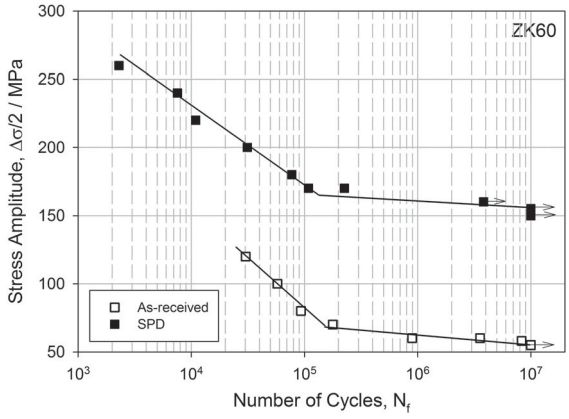

Figure 6. Wöhler plot for Mg alloy ZK60 in the as-received condition (open symbols) and after processing by integrated direct extrusion and ECAP.[63]

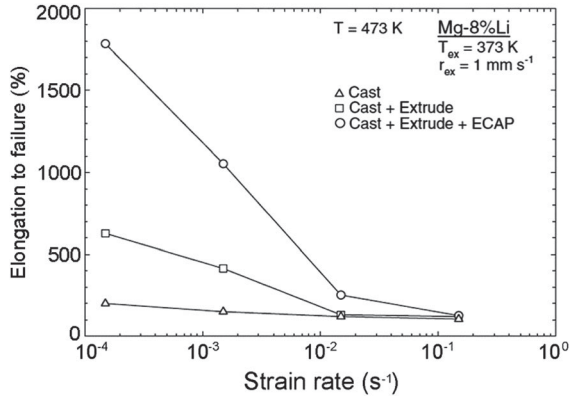

Figure 7. Elongation vs. strain rate at 473 K for a Mg–8% Li alloy in the cast condition, after casting and extrusion, and after casting and extrusion followed by ECAP.[75]

3.3. Superplasticity. Superplasticity refers to the ability of a polycrystalline specimen to pull out to a very high strain, defined typically as an elongation of at least 400%,[68] when tested in tension. The development of a superplastic capability in polycrystalline materials is significant because of the increasing importance of the superplastic-forming industry in the manufacture of complex parts having curved surfaces.[69] Superplasticity requires a small grain size, typically below $\sim 10\ \mu$m, and it is now recognized that the dominant flow process is grain boundary sliding in which the strain rate varies inversely with the grain size raised to a power of 2.[70] This means in practice that the extremely small grain sizes produced by SPD processing provide a possibility for achieving superplastic flow at exceptionally rapid strain rates. This was first demonstrated in early experiments on two commercial aluminum-based alloys where elongations of up to 1,000% were attained at strain rates of 10^{-2} s^{-1}.[71] This result suggests that an SPD material should exhibit a rapid superplastic-forming capability directly after processing and this was demonstrated by using a biaxial gas-pressure-forming facility and blowing a dome in an SPD-processed Al–Mg—Sc alloy in the short period of only 60 s.[72] Experiments also confirmed that the superplastic properties were retained when the material was processed by ECAP and then rolled into a sheet.[73]

Although it is relatively easy to achieve exceptional grain refinement in face-centered cubic metals, the situation becomes more difficult in hexagonal close-packed metals such as magnesium because of the limited number of available slip systems. To overcome these difficulties, a two-step processing route was developed in which some initial grain refinement is introduced through extrusion prior to processing by ECAP.[74] The effect of this procedure is illustrated in Figure 7 where results are shown for a Mg–8% Li alloy tested in tension over a range of strain rates at 473 K in a cast condition, after casting and extrusion and after casting and extrusion followed by processing by ECAP.[75] The changes introduced by these different processing routes are dramatic because the alloy is not superplastic in the cast condition, it is only marginally superplastic after casting and extrusion, but in the cast + extrusion + ECAP condition it is possible to achieve high elongations of up to 1,800%. Using this two-step processing route, it is feasible to achieve excellent superplastic elongations in magnesium alloys and an example is shown in Figure 8 where a ZK60 Mg–Zn–Zr alloy was pulled to failure at an elongation of 3,050%.[76] In practice, even larger superplastic elongations may be attained in aluminum-based alloys processed by ECAP and there is a recent report of an elongation of 4,100% in an Al–Mg–Sc–Zr alloy when tested at 723 K at a strain rate of 5.2×10^{-2} s^{-1}.[77] Finally, it is important to note that, despite the very small cross-sectional areas of the tensile specimens processed by HPT, it is again possible to achieve excellent superplastic properties with an elongation of 1,800% recorded in an HPT-processed Zn–22% Al eutectoid alloy when pulled to failure at 473 K at a strain rate of 1.0×10^{-1} s^{-1}.[78]

4. Functional Properties of BNM Nanostructuring of metals may also enhance various functional properties or produce new physical and chemical properties, thereby making them attractive for innovative engineering and medical applications. This section reviews the features and nature of the unusual functional properties observed in bulk nanostructured materials.

4.1. Electrical Conductivity in Ultrafine-grained Materials. It is well known that Ag, Cu, Au, and Al are metals with high electrical conductivity (111%, 100%, 78%, and 64% International Annealed Copper Standard [IACS], respectively). In addition to high

Downloaded by [University of Southampton] at 06:30 17 February 2016

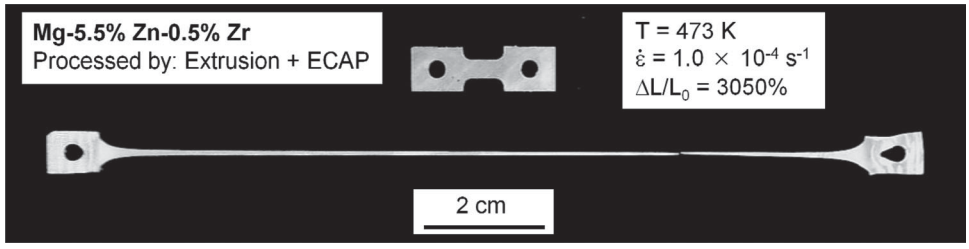

Figure 8. Appearance of a tensile specimen of a ZK60 magnesium alloy pulled to failure at 3,050% after extrusion and ECAP; the upper specimen is untested.[76]

conductivity, high mechanical strength of these metals is required for certain applications. Strengthening is generally achieved through strain hardening, solid-solution hardening, precipitation hardening and grain refinement. However, these strengthening mechanisms also lead to lower conductivity because of electron scattering by crystal lattice defects. Recent studies reveal new ways of solving this problem by grain refinement.

The evolution of mechanical properties and electrical conductivity with strain was investigated for pure Cu processed by ECAP,[79–82] accumulated roll bonding (ARB),[83–85] and HPT.[82] As summarized in Figure 9, in pure Cu (99.99%) the hardness increases and electrical conductivity decreases with increasing equivalent strain in the early stages of straining and both level off to constant levels (130 Vickers hardness, 88% IACS) at equivalent strains exceeding ~20.[82] However, the electrical conductivity decreased by only ~12% whereas the hardness increased by ~270% at this saturation level. Subsequent annealing improved the electrical conductivity to 97% IACS while the hardness increment was maintained at a higher level of ~160% (80 Vickers hardness) when compared to the annealed state (50 Vickers hardness). A Corson alloy was processed by HPT and achieved a high strength (~1 GPa).[86] Furthermore, subsequent aging increased the strength to ~1.1 GPa and improved the electrical conductivity to an acceptable level of ~30% IACS.

The advantageous effects of HPT processing on the strength and electrical conductivity of Cu–0.7%Cr, Cu–0.9%Hf, and Cu–0.7%Cr–0.9%Hf alloys were demonstrated.[87] It was reported that pure copper exhibits a high strength over 1 GPa and an electrical conductivity as high as 97% IACS.[48] The sample was synthesized using a pulsed electrodeposition technique which produced grain sizes of 100–1,000 nm containing a high density of nanotwins. The significance of nanotwinning is that twin boundaries block dislocation motion but have little effect on the electrical resistivity. Such combinations of properties are yet to be matched by SPD processing but the above examples suggest that this is potentially achievable.

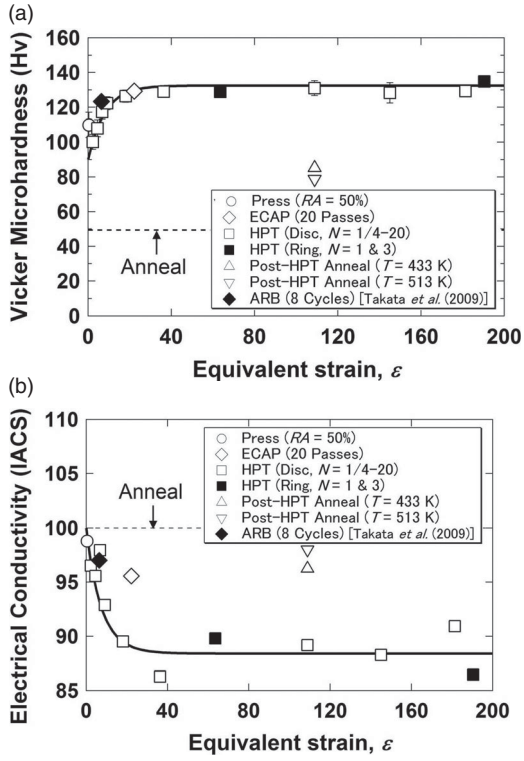

Figure 9. (a) Vickers microhardness and (b) electrical resistivity/conductivity plotted against equivalent strain for samples processed by SPD methods.[82]

Another requirement for electrical conductors is light weight and this is especially important for applications in motors, robots, and power transmission lines. Aluminum is the lightest among the high conductivity metals. It was reported [88,89] that UFG Al–Mg—Si alloys processed by ECAP and HPT exhibit a good combination of increased mechanical properties and enhanced electrical conductivity. The increased conductivity was due to second-phase precipitation which reduced the solute concentration in the Al matrix. It was proposed that processing at elevated temperatures to induce dynamic aging may be promising for continuous wire production.[90] Taking advantage of the low solubility of Fe in Al (~0.05 wt%) and a fine eutectic structure at ~1.8 wt%Fe, an Al–Fe alloy was processed

Downloaded by [University of Southampton] at 06:30 17 February 2016

Downloaded by [University of Southampton] at 06:30 17 February 2016

by HPT and subsequent aging which resulted in a high strength of 600 MPa and a high conductivity of $>50\%$ IACS.[91,92]

4.2. Giant Magnetoresistance (GMR) Produced by HPT. When ferromagnetic particles are finely dispersed in a non-magnetic matrix, magnetoresistance (MR) appears with an isotropic feature. This isotropic MR is called GMR if the MR ratio reaches a magnitude of more than a few tens of percent.[93–100] The Cu–Co system is known as a good candidate for GMR as ferromagnetic Co particles with little solubility of Cu coexists in the Cu matrix.[101] A Cu–10wt%Co alloy was processed using HPT to achieve a fine dispersion of ferromagnetic particles and MR was reported at a level $\sim$2.5% at 77 K with an isotropic feature (Figure 10).[102] The appearance of MR was also confirmed in a Cu–22wt%Fe alloy.[103] While the achieved magnitudes of the MR do not qualify as GMR, the results show that HPT is at least potentially promising for creating GMR in alloys.

4.3. Enhanced Hydrogen Storage Performance of SPD-processed Materials.

4.3.1. Mg and Mg Alloys. Since 2004, ECAP has been used to process nanometals for hydrogen storage, particularly Mg and its alloys (ZK60) (Figure 11).[104–106] The advantages of ECAP over ball milling include prevention of oxidation, which can seriously inhibit absorption/desorption of H_2, and the low production cost as large volumes of material can be efficiently processed using ECAP. Furthermore, ECAP avoids health hazards common to toxicity-prone nanopowder-based processes.

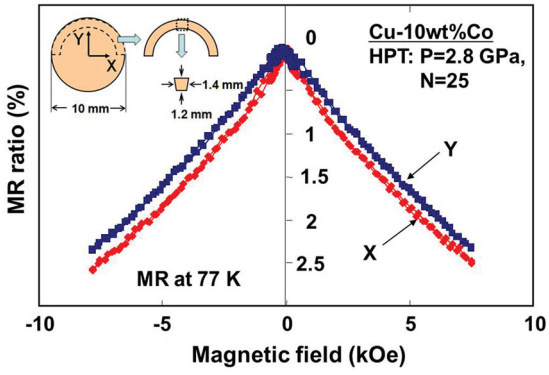

Figure 10. Variation of MR ratio with magnetic field in two different directions (X and Y) for HPT sample after $N = 25$ revolutions, where the definition of X and Y is as illustrated.[102]

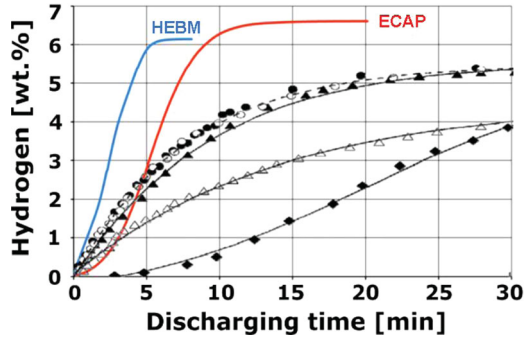

Figure 11. Hydrogen storage kinetics showing high performance of ECAP-processed ZK60 alloy compared to its ball-milled counterpart (desorption,[104,105]).

A critical requirement for energy storage is stability of the storage capacity and the absorption/desorption kinetics over large numbers of cycles. Ball-milled Mg and Mg alloys rarely meet this requirement unless catalysts are added.[107] As seen in Figure 12, ECAP-processed ZK60 shows high stability of both its capacity for hydrogen uptake and the hydrogenation/dehydrogenation kinetics for at least 1,000 cycles.[105] This was also confirmed for HPT-processed ZK60 for at least 100 cycles (Figure 13,[108]). However, not all SPD-processed materials show high stability. There are several reports [109–111] that ARB- or HPT-processed MgH_2 powder has good kinetics but low stability and this was confirmed by a recent high-cycle study [108] as shown in Figure 14. After 40 cycles, the capacity of hydrogen loading clearly decreased. Comparing the long-time stability of SPD-processed materials ZK60 and MgH_2, it was concluded that the SPD processes in both materials provide nucleation sites for hydride formation which are, however, not stable in the case of SPD-processed pure MgH_2. In that material, it is the comparably large volume of the hydride particles which decreases the hydrogen loading capacity as the hydrogen diffusion becomes sluggish compared with the non-hydrogenated substance.[108]

4.3.2. TiFe Alloys. The TiFe intermetallic with B2-type crystal structure is a well-known candidate for stationary hydrogen storage because of its low hydrogenation temperatures, reversible hydrogenation features, high hydrogen storage capacity, and low price. However, its practical application is limited as it requires an activation process before hydrogenation, which includes exposure to hydrogen atmosphere under high pressures at high temperatures. There have been many attempts to overcome this limitation.[112–120] Recent studies have shown that SPD processing is the way to achieve that, as such an activation process is no longer required when the TiFe is pre-processed by

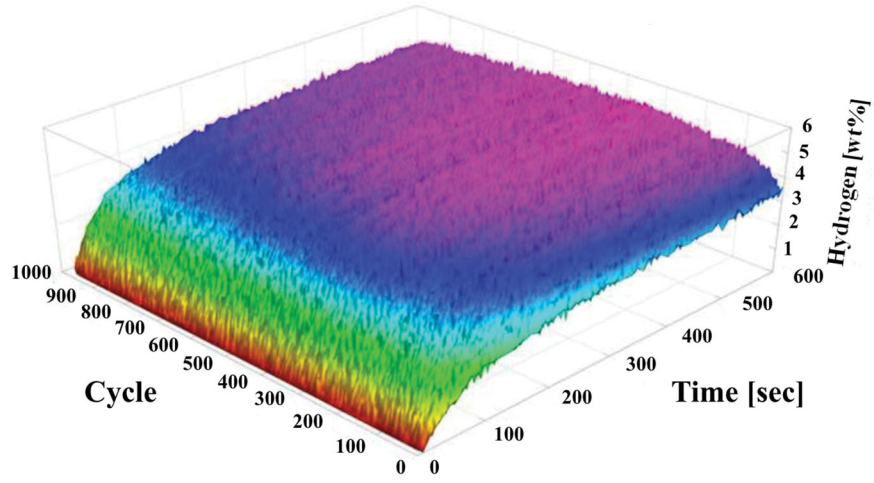

Figure 12. Long time characteristics of hydrogen storage (absorption) measured in the ECAP-processed ZK 60 alloy (from [105]).

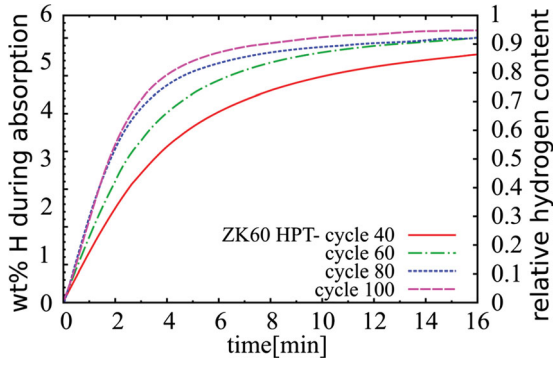

Figure 13. Hydrogen absorption of ZK60 after HPT processing at room temperature after different numbers of cycles of hydrogen loading and unloading, according to [108].

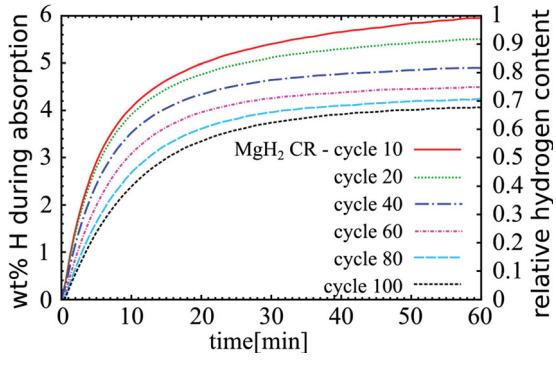

Figure 14. Hydrogen absorption of MgH_2 after cold rolling at room temperature after different numbers of cycles of hydrogen loading and unloading, according to [108].

HPT (Figure 15).[121] Furthermore, the HPT-processed sample is not deactivated even after storage in air for a prolonged period of time.[122] The mechanism enabling hydride formation without activation is associated with enhanced diffusion of hydrogen that occurs via HPT-induced microcracks and nanograin boundaries. A further study on TiFe also showed that plastic straining is important in these hard intermetallics. Another SPD process, specifically groove rolling of encapsulated billets, was shown to be effective in activating TiFe samples as well.[123]

4.4. Production of Nanograins in Semiconductors and Occurrence of Photoluminescence. When crystalline Si is subjected to high pressure, allotropic transformations occur from the diamond cubic structure (Si-I) to high-pressure phases with different crystal structures. These include Si-II with the β-Sn structure, Si-III with body-centered cubic structure, and other phases.[124] Because such high-pressure phases are semi-metallic in nature, they are more likely to deform plastically at room temperature under high pressure. An early study [125] and more recent studies [126,127] reported the formation of nanograins in crystalline Si processed by HPT. The mechanism for the nanograin formation is not understood but it is probably associated with enhanced dislocation activity or transformation-induced grain refinement.[2,128,129] It is interesting to note that nanocrystalline Si (*nc*-Si) exhibits unique optical properties such as visible photoluminescence (PL) because of quantum confinement.[130] It was shown that annealing after HPT gave rise to a reverse transformation of Si-III and Si-XII to Si-I while retaining the nanograined structure (Figure 16).[127] This is reflected in a broad PL peak centered around 600 nm due to the quantum confinement effect in the Si-I nanograins (Figure 17).[127] The application of HPT to Ge and GaAs also produced nanograins [131,132] and a similar PL peak was also observed for GaAs owing to the nanograin formation by HPT processing and subsequent

Downloaded by [University of Southampton] at 06:30 17 February 2016

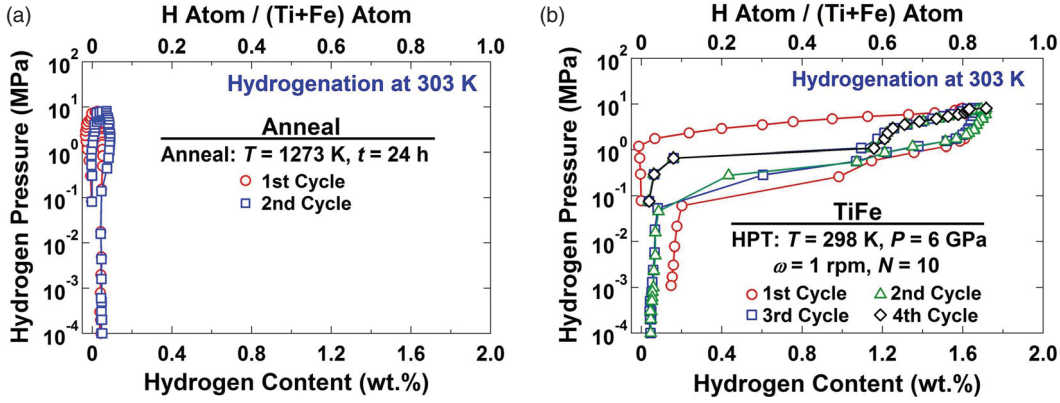

Figure 15. Pressure–concentration (P–C) isotherms at 303 K for samples processed by (a) annealing at 1,273 K for 24 h and (b) HPT processing for 10 turns. Fourth cycle in (b) was terminated after absorption for conducting XRD analysis.[121]

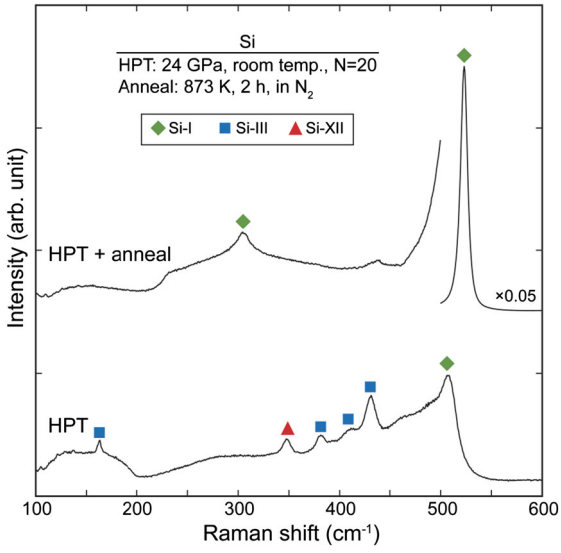

Figure 16. Raman spectra after HPT processing for 20 revolutions and annealing. Each Raman spectrum was taken at about 2 mm from the disk center.[127]

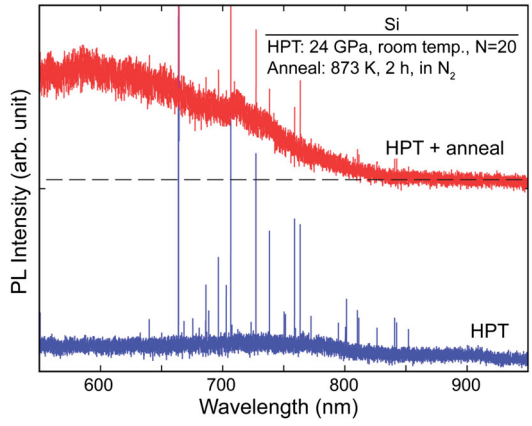

Figure 17. PL spectra after HPT processing for 20 revolutions and annealing. Some of the sharp luminescence peaks are due to laser plasma lines.[127]

annealing.[132] It should be noted that *nc*-Si is commonly produced by ion implantation,[133] electrochemical etching,[134] and chemical vapor deposition,[135] all of which are suitable for low-dimensional nanostructures such as porous Si and Si dots. It is important to emphasize that the nano-grained semiconductors were obtained in *bulk* form by virtue of HPT. Thus, the HPT processing of semiconductors can be of great interest for potential applications to optoelectronic devices.

4.5. Superconductors in Nanograin Structures.

Superconducting properties such as the critical temperature T_c, critical current density J_c, and upper critical field H_{c2} may be affected when the sample size is reduced to the superconducting coherence length (ξ) due to the quantum-confinement effect.[136–138] Although the size effect on the superconducting transition was studied by fabricating an ultrathin lead film [139] and an aluminum nanowire,[140] a recent report [141] examined the effect of grain size on the superconducting properties of bulk polycrystalline Nb whose grain size was reduced to $\sim$250 nm using HPT processing.[142] This grain size is equivalent to $\sim 5\xi$ and the effect was appreciable. It was shown that the values of T_c, J_c, and H_{c2} were increased due to grain refinement by HPT processing (Figure 18). The increase in J_c can be attributed to the enhanced vortex pinning due to crystal lattice defects such as dislocations and grain boundaries. It was also shown that the residual resistivity ρ_0 is governed by the amount of strain imposed by the HPT processing.

Superconductivity was also studied for a well-known system used for superconducting magnets, a Nb-47wt%Ti alloy, to examine the effect of HPT processing on T_c.[143] It was found that T_c occurred below 9 K, it decreased with increasing shear strain but rose again with annealing. Although the grain size of the material was comparable with the coherence length (about 8ξ),[144] the trend of T_c with the imposed strain was

Downloaded by [University of Southampton] at 06:30 17 February 2016

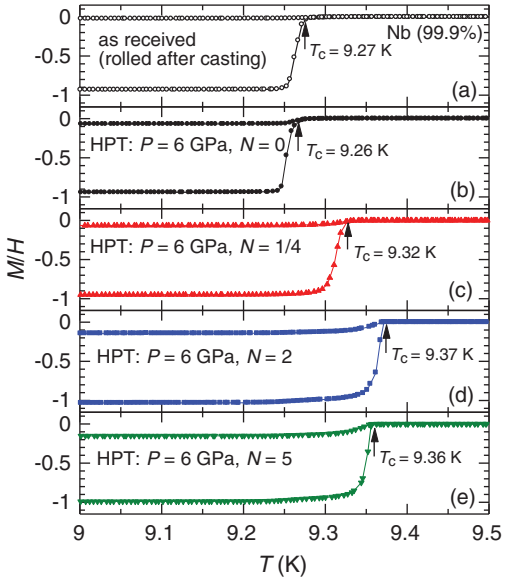

Figure 18. Temperature dependence of the magnetization $M(T)$ of Nb in the magnetic field $H = 2$ Oe. (a) As-received sample; (b)–(e) HPT-processed samples with different revolution numbers N.[141]

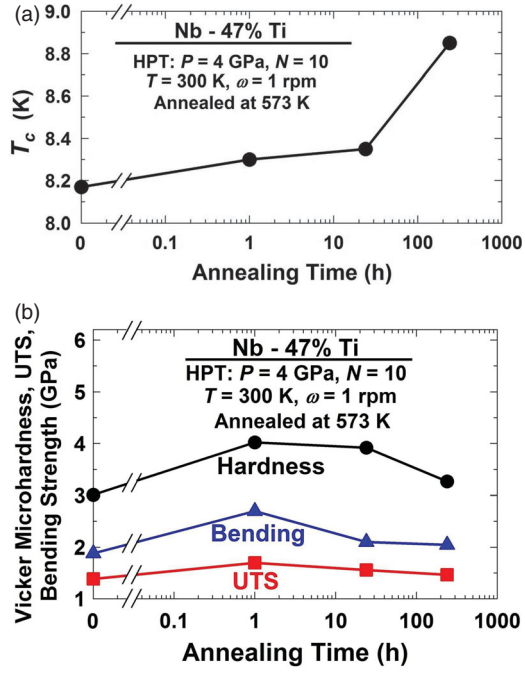

Figure 19. Variation of (a) transition temperature for superconductivity, T_c, and (b) Vickers microhardness, UTS, and bending strength against annealing time for samples processed by HPT for $N = 50$ turns and annealed at 573 K.[143]

opposite to pure Nb [141] and this was attributed to dissolution of Ti in Nb with straining by HPT. The increase in T_c upon annealing was due to Ti decomposition from a supersaturated state after HPT processing. An important conclusion is that the application of the HPT processing to the Nb-47wt%Ti alloy in conjunction with subsequent annealing leads to an increase in tensile strength as well as bending strength while also maintaining T_c above the value obtained after solution treatment (Figure 19).

4.6. Thermoelectrics. In the field of thermoelectrics, so far mainly two groups of materials were considered in the context of SPD processing (for a detailed review, see [145]): (i) Bi–Te alloys for low-temperature applications and (ii) skutterudites for high-temperature applications. The successes of SPD processing can be judged upon the efficiency of processed thermoelectrics in terms of the so-called figure-of-merit:

$$\mathrm{ZT} = \frac{S^2 T}{\rho\lambda}. \qquad (4)$$

A large ZT-value is reached either via a high thermovoltage represented by the Seebeck coefficient S or by a decrease in electrical resistivity ρ as well as a decrease in the thermal conductivity λ. The S-value can be enhanced by increasing the gradient of the density of states, for example, by limiting the sample dimensions to a few nanometers or even to the atomic scale as in topological semiconductors, like graphene or silicon [146]). As such dimensions are usually not reached in SPD processing, efforts so far have concentrated on the decrease of ρ and λ. Now the problem arises of controlling these two quantities independently. This problem needs to be tackled individually for the two groups of materials considered.

The *low-temperature thermoelectric Bi–Te alloys* exhibit a large crystal anisotropy which means that the texture of the SPD-processed materials is even more important for the resultant ZT value than the decrease in grain size leading to a smaller thermal conductivity through additional phonon scattering. There have been several attempts to increase ZT by application of SPD, mainly HPT [147] and ECAP.[148] HPT processing gave rise to an increased power factor S^2/ρ due to a (110) texture contributing to both a low resistivity and a high Seebeck coefficient (Figure 20,[147]). A real increase in ZT by an SPD method was achieved by the ECAP procedure [148] by carefully choosing the ECAP temperature (773 K) and path (Route A where there is a rotation of the billet by 180° after each pass) in order to obtain high carrier mobility (Figure 21), thus minimizing the electrical resistivity and thereby achieving a figure of merit as high as ZT = 2.3.

From among *high-temperature thermoelectrics*, so far *skutterudites* have been the subject of SPD processing. Ball-milled skutterudite nanopowder was successfully consolidated by means of HPT at a distinctly lower temperature than the conventional hot pressing, thus yielding much smaller grain sizes.[149] It was found that the thermal conductivity was strongly decreased by

Downloaded by [University of Southampton] at 06:30 17 February 2016

Downloaded by [University of Southampton] at 06:30 17 February 2016

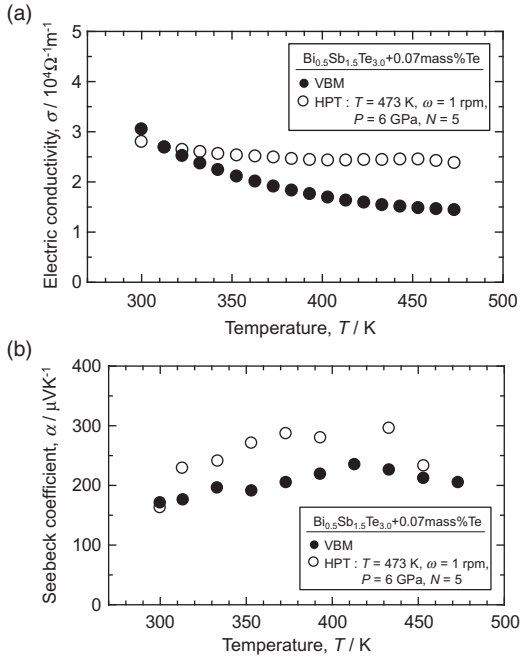

Figure 20. Electrical conductivity (a) and Seebeck coefficient (b) vs. temperature, for *p*-type $Bi_{0.5}Sb_{1.5}Te_{3.0}$ after processing by the Vertical Bridgman Method and HPT.[147]

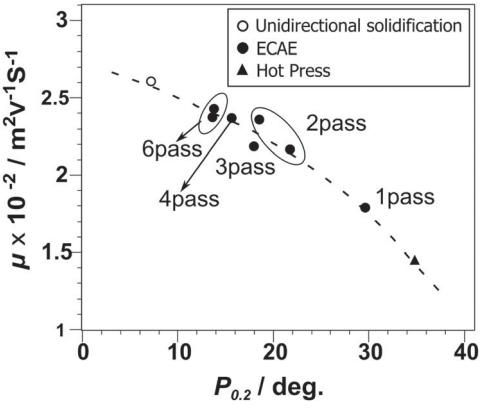

Figure 21. Dependence of carrier mobility μ on preferred orientation angle $P_{0.2}$, after applying different numbers of passes of Route A ECAP (labeled 'ECAE' in the original figure (from [148]).

HPT-induced lattice defects although cracks and voids were also generated and increased the electrical resistivity far more so that the overall ZT dropped. This problem was addressed by suitably increasing the HPT processing temperature in order to avoid the formation of cracks and voids, thus keeping the increase in resistivity sufficiently low to achieve an overall increase in ZT (Figure 22).[145,150] By optimizing the HPT-processing temperature, pressure, and strain, ZT was further increased by a factor of 2–3 ([145,150]; Figure 22) compared with the value before HPT. Finally, with ZT = 1.9, a world record for *n*-type skutterudites was set using this strategy

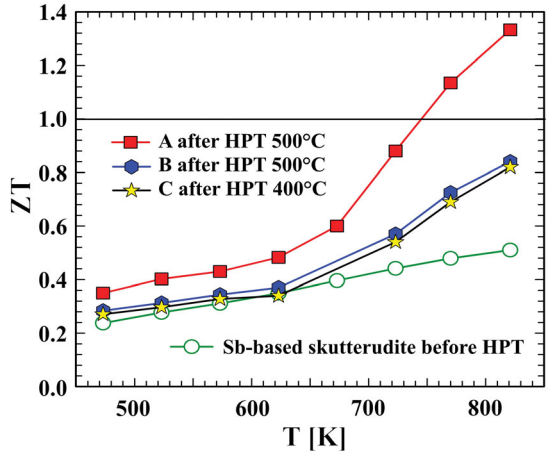

Figure 22. Increase in ZT in an *n*-type skutterudite after HPT processing at temperatures 400°C and 500°C. Letters A, B, and C refer to different strains achieved by HPT (from [145]).

([151]; Figure 23). Most recently, another world record ZT = 1.45 was also established for *p*-type skutterudites [152] by means of a similar preparation procedure. It should be mentioned that this procedure does not introduce new phases,[153] unlike in many alloys processed by SPD,[154] and instead there are changes only in the density and arrangement of SPD-induced crystal lattice defects.[153] Among the latter, there clearly were some which increased the electrical resistivity but without decreasing the lattice thermal conductivity. It must be left to further research whether, in the interest of maximizing ZT, it is possible to remove such defects without losing those that significantly reduce λ.

4.7. SPD-processed Materials in Biomedical Applications. One application where SPD technologies have achieved one of their most significant successes is the area of medical implant materials. The contemporary development of metallic implant materials is driven by the need for improved mechanical performance and biocompatibility. Different paradigms govern this development for permanent and temporary (bioresorbable) implants. While materials for permanent implants, such as bone or tooth replacement, obviously need to be as inert as possible, those for temporary implants are required to degrade at a rate commensurate with the rate of tissue healing. Various materials are being explored as candidates for such applications with an aim to improve their properties by SPD processing.[155] The archetypal alloy systems that offer the best performance for these two kinds of applications are arguably those based on titanium and magnesium. Indeed, Ti forms a protective surface layer of titania and is considered to be bio-inert (thus being suitable for permanent implants) whilst Mg is very reactive and biodegradable.

Downloaded by [University of Southampton] at 06:30 17 February 2016

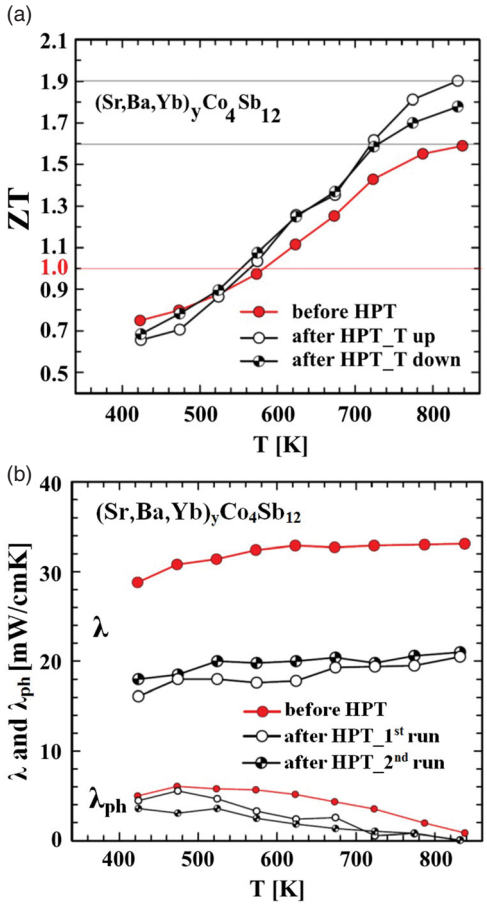

Figure 23. (a) Increase in ZT to a world record ZT = 1.9 by HPT processing; the increase is mainly due to the decrease in thermal lattice conductivity λ_{ph} shown in (b) [151]

For titanium-based alloys, among which Ti-6Al-4V is currently most used, a great challenge is the real or perceived toxicity of the alloying elements. Commercial purity titanium grades are thus becoming the materials of choice. To compensate for the loss of strength associated with alloying, SPD techniques are employed, such as ECAP and, recently, its continuous modification ECAP-Conform.[66,155–158] In this way, extreme grain refinement, almost down to the nano scale, is attained, and this leads to an enhancement of tensile strength of pure titanium to the levels of the conventional alloy Ti-6Al-4V and higher with UTS > 1,300 MPa.[66,156,158] Similar encouraging results were obtained for the fatigue strength and this makes it possible to improve the design of medical implants with better functionality (Figure 24).[156,158] Recent reviews compile the results obtained by ECAP, as well as by more involved SPD processing routes.[66,155] It is especially encouraging that biocompatibility of Ti does not suffer from the ultrafine crystallinity.[159] On the contrary, enhanced rates of attachment and proliferation of osteoblast and fibroblast cells, as well as stem

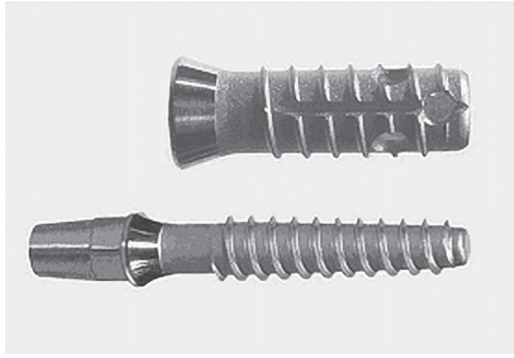

Figure 24. 3.5 mm diameter Timplant® (above) and the new 2.4 mm diameter Nanoimplant® produced from superstrong *n*-Ti (below).[156,158]

cells,[156,157,160] were obtained in a number of *in vitro* assays. *In vivo* studies, while not confirming such enhancement, demonstrated that a spectacular improvement of the mechanical performance of ECAP-modified commercial purity Ti was not accompanied by a loss of biocompatibility.[161]

To further improve biocompatibility, it has been attempted (i) to replace Al and especially V with more biocompatible elements and (ii) to make Young's modulus close to that of bone in order to avoid the so-called 'stress shielding'.[162] In particular, Ti–Nb alloys have attracted a great deal of interest. Not only do they meet both these requirements, but they also show good biocorrosion properties.[162] However, since a low Young's modulus is inherently connected with a relatively low strength, some additional strengthening is required if this material is to be used for medical applications as in implants or prostheses. Processing by SPD can improve the strength via grain refinement.[163–168] However, due to the potential of SPD processing to change phase stability as a result of shear combined with hydrostatic pressure, additional phases may form and this may produce undesired changes—mostly increases—of the overall Young's modulus (see, e.g.[166]) except when a new phase has a low Young's modulus too.[167] Also, SPD processing of ternary and quaternary alloys obtained by replacing some of the Nb content by other constituents such as Ta, Zr, and Sn may affect the Young's modulus in a similar way. Nevertheless, if care is taken in choosing the SPD parameters, such as limited pressure and strain, as well as the number and type of alloy constituents, the strength may be increased by 30–120% (Figures 25 and 26,[157,168]). The selection of an SPD method is also important if a good ductility is required for the intended application. Hydro-Extrusion (HE) may be the SPD method of choice, thereby sacrificing some strength for higher ductility. It is important to emphasize that with all different SPD methods applied to date (Rolling and Folding (R & F), HE, and HPT [168]),

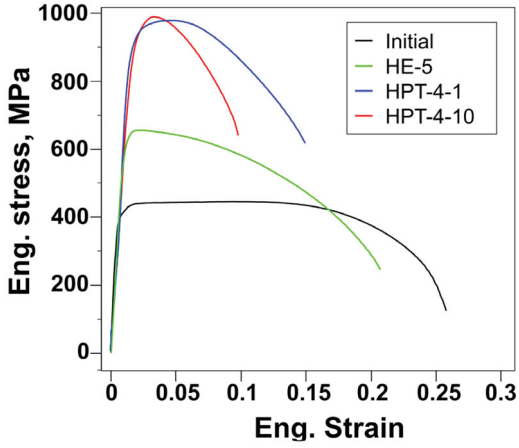

Figure 25. Stress–strain curves for initial and SPD-processed Ti-45Nb samples. HE-5 stands for 97% area reduction by HE, HPT-4-X for High-Pressure Torsion at a pressure of 4 GPa and X revolutions.[168]

a low Young's modulus was maintained (Figure 26). Smaller changes may happen according to the texture evolution which, again, is specific to the particular SPD method chosen ([168]; Figure 26). While with HPT processing the evolving texture is weak, this is not so for the R & F technique, the Young's modulus becoming even lower than initially, so that the elastic behavior of the material is closer to that of bone.

Magnesium is very promising for medical applications because of its light weight and bioresorbability. [169,170] As the lightest of all structural metals (except beryllium), the use of magnesium can reduce the weight of many medical structures from wheelchairs and stretchers to surgical tools, to vascular stents and orthopedic implants.[171,172] Magnesium is also among the most biocompatible of metals.

The prospect of nanostructuring magnesium and its alloys to achieve novel properties was recognized more than 20 years ago.[2,173,174] Grain refinement has been regarded as one of the most attractive methods to enhance the performance of magnesium alloys.[175] In addition to grain refinement, substantial texture effects are induced in hcp magnesium alloys by SPD processing. The latter are sometimes sufficiently large to introduce significant mechanical anisotropy, and they are large enough in magnitude to cause net softening upon ECAP [176,177] which is to be avoided through appropriate process design.

Nanostructuring of magnesium alloys offers several advantages and alternatives for biomedical applications, for example in vascular stents. First, reducing the grain size alters the corrosion rate. An AZ31 alloy was processed by ECAP and it was found that the corrosion rate in Hank's solution was reduced, although not sufficiently to make it suitable for stent applications.[178] An AZ80 alloy was deformed by ECAP and extrusion to

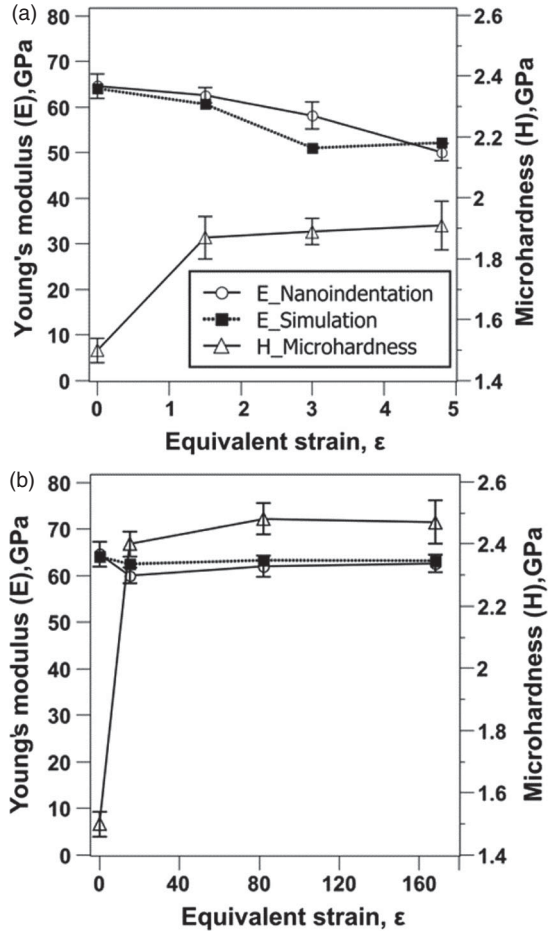

Figure 26. Young's modulus E as measured by nanoindentation (open circles), and microhardness H (open triangles), as a function of von Mises equivalent strain ϵ, for R & F (a) and HPT samples (b). The values of E were also calculated from texture data (full squares).[168]

obtain an UFG structure that enhanced the electrochemical properties.[179] The polarization layers produced remained stable and completely resisted degradation for up to 96 h. More recently, the electrochemical characteristics of AE21 and AE42 alloys were evaluated after processing by ECAP for eight passes.[180] It was found that the smaller grain size resulting from ECAP enhanced the corrosion rate in AE21 due to increased chemical activity at the grain boundaries whereas, by contrast, the corrosion rate in AE42 was reduced after the same ECAP treatment. In the latter case, the larger effect of increased uniformity of the spatial distribution of alloying elements offsets the effect of a smaller grain size. Clearly, the effects of nanostructuring are complex and alloy dependent and accordingly they must be carefully evaluated for any prospective magnesium alloy.

In particular, osteoconductive characteristics of nanostructured surfaces need further exploration. The *in vivo* characteristics of both conventional and nanostructured magnesium alloys need to be researched to

Downloaded by [University of Southampton] at 06:30 17 February 2016

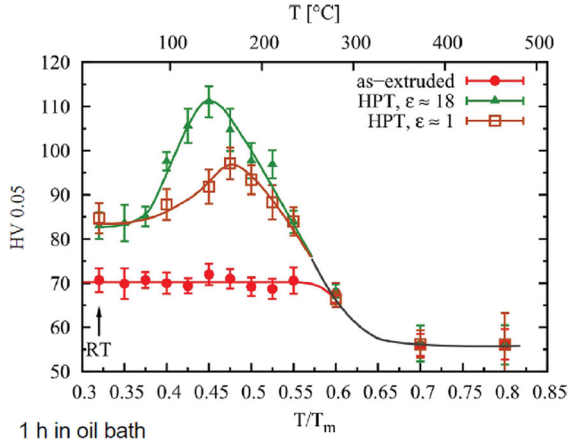

Figure 27. Microhardness of samples of Mg0.2Zn0.5Ca as a function of homologous annealing temperature T/T_m (T and T_m denoting the annealing temperature and the melting temperature in Kelvin, respectively): (i) after 1 h annealing (full circles) and (ii) after HPT processing and annealing (squares and triangles). HPT processing was done at a pressure of 4 GPa up to von Mises equivalent strains ϵ indicated.[183]

establish the basis for realizing the high potential of magnesium-based stents and orthopedic devices.

As noted earlier, the ability of Mg to be resorbed in bodily fluids makes it a good candidate for biodegradable implants. Various Mg alloys have been tested with respect to their biodegradability. Mg–Zn–Ca alloys have proven to exhibit two advantages at the same time, a good biodegradability and high strength.[181] However, recent experiments with these alloys show that, with respect to the time necessary for tissue healing, these alloys may either degrade too quickly and/or the concomitant hydrogen evolution is faster than the organism can absorb. It was found that the lower the alloying element and/or impurity content of the Mg-alloy, the longer it takes for the alloy to degrade.[182] On the other hand, this means that the potential of the alloy for high strength becomes smaller because second-phase particles cannot form and also solid-solution hardening becomes insignificant. It also becomes harder to reduce the grain size of the Mg alloy below 1 μm with the presence of fewer second-phase particles and/or atoms in solid solution. Very recently, it was reported that strengthening of Mg and its dilute alloys can be affected by the agglomeration of surplus vacancies in vacancy clusters or loops.[183] Figure 27 presents this strengthening effect for the case of biodegradable alloy Mg0.2Zn0.5Ca, which was HPT processed to generate vacancies [184,185] and annealed at homologous temperatures up to about 0.5 T_m (where T_m is the melting temperature in Kelvin) in order to induce agglomeration of these vacancies. Depending on the HPT strain applied, the strength increment amounted to almost 60% of the strength of the as-extruded material (Figure 27). By comparison, grain size strengthening yielded a strength increment of only 19% and this is irrespective of the HPT strain applied (Figure 27;[183]). The hypothesis that vacancies are responsible for the observed strengthening effect is supported by two facts, namely that (i) very similar hardening effects with respect to extent and annealing treatment have been reported for quenched-in vacancies [186] and (ii) careful checks by Atom Probe Tomography [183] ruled out the formation of a second phase as an alternative cause for strengthening.

5. Summary The results of numerous studies reported in this article demonstrate clearly that various superior properties, both mechanical and functional, can be obtained in bulk nanostructured materials produced by SPD. The results of numerous studies reported in this article demonstrate clearly that various superior properties, both mechanical and functional, can be obtained in bulk nanostructured materials by SPD. The basic mechanical properties considered include superior strength, enhanced fatigue endurance, and superplasticity. These studies generate a great deal of interest with regard to scientific foundations of the phenomena involved and their practical applications in new structural materials. Recent discoveries have also demonstrated new opportunities for SPD processing with respect to improving functional properties of materials. These include increased electrical conductivity in metals and alloys, giant magnetoresistance, enhanced hydrogen storage performance, occurrence of photoluminescence in nanograined semiconductors, superior thermoelectric properties, and many other unique phenomena that are of immediate interest for various functional applications.

Observations performed during the last decade with a suite of modern techniques including TEM/HREM, X-ray diffraction, 3D-atom probe, and others reveal that not only can SPD processing form UFGs but it can also be used to engineer grain boundary structure and generate nanoparticles, segregations or nanoclusters and other structural elements at nano scale. The type and morphology of such nanostructured elements, as well as their number density, determine new deformation and transport mechanisms responsible for improvement of mechanical, chemical and physical properties of bulk nanostructured materials through SPD techniques.

Over the last few years, studies of bulk nanostructured materials tend to be oriented more toward the development of their advanced and superior properties and in this context the concept of nanostructural design plays an important role. In addition to grain refinement down to the nanometer range, grain boundary structure engineering is also important because boundaries having different structures can exhibit specific transport mechanisms, in terms of deformation and diffusion, and this can be used to control the properties.[7,187] This opens up the potential for developing new ways for improving the properties of ultrafine-grained materials.

Downloaded by [University of Southampton] at 06:30 17 February 2016

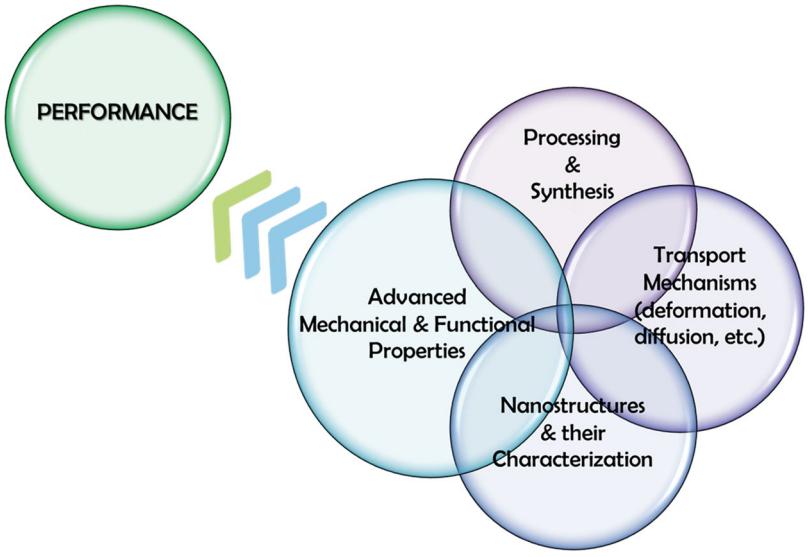

Figure 28. Principles of nanostructural design of bulk nanostructured materials.[5]

The concept of the nanostructural design of materials is schematically illustrated in Figure 28 [5] using a pictorial representation which modifies and further develops the well-known concept of the contemporary creation of novel materials through the integration of theory and modeling, structure characterization, processing and synthesis, as well as studies of the properties. In comparison with traditional materials design, nanostructuring of bulk materials deals with a far larger number of structural parameters related to the grain size and shape, lattice defects in the grain interior, as well as with rich grain boundary structure, and also with the presence of segregations and second-phase nanoparticles. This provides the possibility to vary the transport mechanisms and change the properties of materials in a desired way. Not only does nanostructuring of bulk materials by SPD processing permits a considerable enhancement of mechanical and physical properties, but it may also be used to create multifunctional materials.[4,8,9,31,188,189] In this respect, it can be anticipated that in the very near future the nanostructuring of materials by SPD processing techniques under different controlled regimes will provide new breakthroughs in the development of materials with superior properties for advanced structural and functional applications.

Disclosure Statement No potential conflict of interest was reported by the authors.

Acknowledgements This work was partially supported by the Russian Federal Ministry for Education and Science (through RZV Grant No. 14.B25.31.0017 and YE Grant No. 14.A12.31.0001); the Light Metals Educational Foundation of Japan, Grant-in-Aid for Scientific Research S (No. 26220909) and in Innovative Areas 'Bulk Nanostructured Metals' (No. 22102004) from the MEXT, Japan (ZH) and the European Research Council under ERC Grant Agreement No. 267464-SPDMETALS (TGL). Further support by the EU-ITN BIOTINET under Grant Agreement No. 264635 is gratefully acknowledged (MZ).YTZ is funded by the US Army Research Office (W911 NF-12-1-0009), the National Science Foundation of the United States (Grant No. DMR-1104667) and the China 1000 Plan program.

References

[1] Valiev RZ, Langdon TG. Report of international NanoSPD steering committee and statistics on recent NanoSPD activities. IOP Conf Ser Mater Sci Eng. 2014;63:011002.
[2] Valiev RZ, Islamgaliev RK, Alexandrov IV. Bulk nanostructured materials from severe plastic deformation. Prog Mater Sci. 2000;45:103–189.
[3] Valiev RZ, Estrin Y, Horita Z, Langdon TG, Zehetbauer MJ, Zhu YT. Producing bulk ultrafine-grained materials by severe plastic deformation. J Mater. 2006;58: 33–39.
[4] Zehetbauer MJ, Zhu YT, editor. Bulk nanostructured materials. Weinheim: Wiley-VCH; 2009.
[5] Valiev RZ, Zhilyaev AP, Langdon TG. Bulk nanostructured materials: fundamentals and applications. Hoboken, NJ: Wiley; 2014.
[6] Wang YB, Liao XZ, Zhao YH, Cooley JC, Horita Z, Zhu YT. Elemental separation in nanocrystalline Cu-Al alloys. Appl Phys Lett. 2013;102:231912.
[7] Langdon TG. Twenty-five years of ultrafine-grained materials: achieving exceptional properties through grain refinement. Acta Mater. 2013;61:7035–7059.
[8] Production of multifunctional materials using severe plastic deformation. In: Horita Z, Editor. International Symposium on Giant Straining Process for Advanced Materials (GSAM2010). Fukuoka: Kyushu University Press; 2010.

Downloaded by [University of Southampton] at 06:30 17 February 2016

Downloaded by [University of Southampton] at 06:30 17 February 2016

[9] Estrin Y, Vinogradov A. Extreme grain refinement by severe plastic deformation: a wealth of challenging science. Acta Mater. 2013;61:782–817.

[10] Sauvage X, Wilde G, Divinski SV, Horita Z, Valiev RZ. Grain boundaries in ultrafine grained materials processed by severe plastic deformation and related phenomena. Mater Sci Eng A. 2012;540:1–12.

[11] Zhu YT, Liao XZ, Wu XL. Deformation twinning in nanocrystalline materials. Prog Mater Sci. 2012;57: 1–62.

[12] Zhao YH, Bingert JE, Liao XZ, et al. Simultaneously increasing the ductility and strength of ultra-fine-grained pure copper. Adv Mater. 2006;18:2949–2953.

[13] Zhao YH, Liao XZ, Cheng S, Ma E, Zhu YT. Simultaneously increasing the ductility and strength of nanostructured alloys. Adv Mater. 2006;18:2280–2283.

[14] Zhao YH, Zhu YT, Liao XZ, Horita Z, Langdon TG. Tailoring stacking fault energy for high ductility and high strength in ultrafine grained Cu and its alloy. Appl Phys Lett. 2006;89:121906.

[15] Zhilyaev AP, Langdon TG. Using high-pressure torsion for metal processing: fundamentals and applications. Prog Mater Sci. 2008;53:893–979.

[16] Valiev RZ, Langdon TG. Principles of equal-channel angular pressing as a processing tool for grain refinement. Prog Mater Sci. 2006;51:881–981.

[17] Wu XL, Zhu YT. Inverse grain-size effect on twinning in nanocrystalline Ni. Phys Rev Lett. 2008;101:025503.

[18] Zhu YT, Liao XZ, Wu XL, Narayan J. Grain size effect on deformation twinning and detwinning. J Mater Sci. 2013;48:4467–4475.

[19] Ni S, Wang YB, Liao XZ, et al. Effect of grain size on the competition between twinning and detwinning in nanocrystalline metals. Phys Rev B. 2011;84:235401.

[20] Nurislamova G, Sauvage X, Murashkin M, Islamgaliev R, Valiev R. Nanostructure and related mechanical properties of an Al-Mg-Si alloy processed by severe plastic deformation. Philos Mag Lett. 2008;88: 459–466.

[21] Sha G, Wang YB, Liao XZ, Duan ZC, Ringer SP, Langdon TG. Influence of equal-channel angular pressing on precipitation in an Al-Zn-Mg-Cu alloy. Acta Mater. 2009;57:3123–3132.

[22] Liddicoat PV, Liao XZ, Zhao YH, et al. Nanostructural hierarchy increases the strength of aluminum alloys. Nature Comm. 2010;1:1–7.

[23] Valiev RZ, Enikeev NA, Murashkin MY, Kazykhanov VU, Sauvage X. On the origin of the extremely high strength of ultrafine-grained Al alloys produced by severe plastic deformation. Scripta Mater. 2010;63:949–952.

[24] Valiev RZ, Murashkin MY, Bobruk EV, Raab GI. Grain refinement and mechanical behavior of the Al alloy, subjected to the new SPD technique. Mater Trans. 2009;50:87–91.

[25] Zhao YH, Zhu YT, Lavernia EJ. Strategies for improving tensile ductility of bulk nanostructured materials. Adv Eng Mater. 2010;12:769–778.

[26] Gertsman VY, Valiev RZ, Akhmadeev NA, Mishin OV. Deformation behaviour of ultrafine-grained materials. Mater Sci Forum. 1996;225–227:739–744.

[27] Gertsman VY, Birringer R, Valiev RZ, Gleiter H. On the structure and strength of ultrafine-grained copper produced by severe plastic-deformation. Scripta Metall Mater. 1994;30:229–234.

[28] Valiev RZ, Korznikov AV, Mulyukov RR. Structure and properties of ultrafine-grained materials produced by severe plastic-deformation. Mater Sci Eng A. 1993;168:141–148.

[29] Segal VM, Ferrasse S, Alford F. Tensile testing of ultra fine grained metals. Mater Sci Eng A. 2006;422:321–326.

[30] Baik SC, Hellmig RJ, Estrin Y, Kim HS. Modeling of deformation behavior of copper under equal channel angular pressing. Zeitschrift Fuer Metallkunde. 2003;94:754–760.

[31] Sabirov I, Murashkin MY, Valiev RZ. Nanostructured aluminium alloys produced by severe plastic deformation: new horizons in development. Mater Sci Eng A. 2013;560:1–24.

[32] Abramova MM, Enikeev NA, Valiev RZ, et al. Grain boundary segregation induced strengthening of an ultrafine-grained austenitic stainless steel. Mater Lett. 2014;136:349–352.

[33] Nanostructured metals and alloys: processing, micro structure, mechanical properties and applications. Oxford: Woodhead; 2011.

[34] Renk O, Hohenwarter A, Eder K, Kormout KS, Cairney JM, Pippan R. Increasing the strength of nanocrystalline steels by annealing: is segregation necessary? Scripta Mater. 2015;95:27–30.

[35] Ahn B, Zhilyaev AP, Lee HJ, Kawasaki M, Langdon TG. Rapid synthesis of an extra hard metal matrix nanocomposite at ambient temperature. Mater Sci Eng A. 2015;635:109–117.

[36] Kim HS, Ryu WS, Janecek M, Baik SC, Estrin Y. Effect of equal channel angular pressing on microstructure and mechanical properties of IF steel. Adv Eng Mater. 2005;7:43–46.

[37] Zhu YT, Liao XZ. Nanostructured metals —retaining ductility. Nature Mater. 2004;3:351–352.

[38] Hart EW. Theory of tensile test. Acta Metall. 1967;15:351–355.

[39] Kim HS, Estrin Y. Ductility of ultrafine grained copper. Appl Phys Lett. 2001;79:4115–4117.

[40] Zhang X, Wang H, Scattergood RO, et al. Studies of deformation mechanisms in ultra-fine-grained and nanostructured Zn. Acta Mater. 2002;50:4823–4830.

[41] Zhang X, Wang H, Scattergood RO, et al. Tensile elongation (110%) observed in ultrafine-grained Zn at room temperature. Appl Phys Lett. 2002;81:823–825.

[42] Valiev RZ, Alexandrov IV, Zhu YT, Lowe TC. Paradox of strength and ductility in metals processed by severe plastic deformation. J Mater Res. 2002;17:5–8.

[43] Hoeppel HW, Zhou ZM, Mughrabi H, Valiev RZ. Microstructural study of the parameters governing coarsening and cyclic softening in fatigued ultrafine-grained copper. Philos Mag A. 2002;82:1781–1794.

[44] Wang YM, Chen MW, Zhou FH, Ma E. High tensile ductility in a nanostructured metal. Nature. 2002;419: 912–915.

[45] Youssef KM, Scattergood RO, Murty KL, Horton JA, Koch CC. Ultrahigh strength and high ductility of bulk nanocrystalline copper. Appl Phys Lett. 2005;87: 091904.

[46] Mungole T, Kumar P, Kawasaki M, Langdon TG. A critical examination of the paradox of strength and ductility in ultrafine-grained metals. J Mater Res. 2014;29: 2534–2546.

Downloaded by [University of Southampton] at 06:30 17 February 2016

[47] Mungole T, Kumar P, Kawasaki M, Langdon TG. The contribution of grain boundary sliding in tensile deformation of an ultrafine-grained aluminum alloy having high strength and high ductility. J Mater Sci. 2015;50:3549–3561.

[48] Lu L, Shen YF, Chen XH, Qian LH, Lu K. Ultrahigh strength and high electrical conductivity in copper. Science. 2004;304:422–426.

[49] Lu K, Lu L, Suresh S. Strengthening materials by engineering coherent internal boundaries at the nanoscale. Science. 2009;324:349–352.

[50] Zhao YH, Liao XZ, Horita Z, Langdon TG, Zhu YT. Determining the optimal stacking fault energy for achieving high ductility in ultrafine-grained Cu-Zn alloys. Mater Sci Eng A. 2008;493:123–129.

[51] Cheng S, Zhao YH, Zhu YT, Ma E. Optimizing the strength and ductility of fine structured 2024 Al alloy by nano-precipitation. Acta Mater. 2007;55: 5822–5832.

[52] Zhao YH, Bingert JF, Zhu YT, et al. Tougher ultrafine grain Cu via high-angle grain boundaries and low dislocation density. Appl Phys Lett. 2008;92:081903.

[53] Valiev RZ, Murashkin MY, Kilmametov A, Straumal B, Chinh NQ, Langdon TG. Unusual super-ductility at room temperature in an ultrafine-grained aluminum alloy. J Mater Sci. 2010;45:4718–4724.

[54] Wu XL, Jiang P, Chen L, Yuan FP, Zhu YTT. Extraordinary strain hardening by gradient structure. Proc Natl Acad Sci USA. 2014;111:7197–7201.

[55] Wu XL, JIang P, Chen L, Zhang JF, Yuan FP, Zhu YT. Synergetic strengthening by gradient structure. Mater Res Lett. 2014;2:185–191.

[56] Lu K. Making strong nanomaterials ductile with gradients. Science. 2014;345:1455–1456.

[57] Fang TH, Li WL, Tao NR, Lu K. Revealing extraordinary intrinsic tensile plasticity in gradient nano-grained copper. Science. 2011;331:1587–1590.

[58] Mughrabi H, Hoeppel HW. Cyclic deformation and fatigue properties of very fine-grained metals and alloys. Int J Fatigue. 2010;32:1413–1427.

[59] Estrin Y, Vinogradov A. Fatigue behaviour of light alloys with ultrafine grain structure produced by severe plastic deformation: An overview. Int J Fatigue. 2010;32:898–907.

[60] Vinogradov A, Ishida T, Kitagawa K, Kopylov VI. Effect of strain path on structure and mechanical behavior of ultrafine grain Cu-Cr alloy produced by equal-channel angular pressing. Acta Mater. 2005;53: 2181–2192.

[61] Vinogradov A, Patlan V, Suzuki Y, Kitagawa K, Kopylov VI. Structure and properties of ultra-fine grain Cu-Cr-Zr alloy produced by equal-channel angular pressing. Acta Mater. 2002;50:1639–1651.

[62] Orlov D, Raab G, Lamark TT, Popov M, Estrin Y. Improvement of mechanical properties of magnesium alloy ZK60 by integrated extrusion and equal channel angular pressing. Acta Mater. 2011;59:375–385.

[63] Vinogradov A, Orlov D, Estrin Y. Improvement of fatigue strength of a Mg-Zn-Zr alloy by integrated extrusion and equal-channel angular pressing. Scripta Mater. 2012;67:209–212.

[64] Ueno H, Kakihata K, Kaneko Y, Hashimoto S, Vinogradov A. Enhanced fatigue properties of nanostructured austenitic SUS 316L stainless steel. Acta Mater. 2011;59:7060–7069.

[65] Medvedev A, Ng HP, Lapovok R, Estrin Y, Lowe TC, Anumalasetty VN. Comparison of laboratory-scale and industrial-scale equal channel angular pressing of commercial purity titanium. Mater. Lett. 2015;145:308–311.

[66] Figueiredo RB, Barbosa ERD, Zhao XC, et al. Improving the fatigue behavior of dental implants through processing commercial purity titanium by equal-channel angular pressing. Mater Sci Eng A. 2014;619: 312–318.

[67] Hoeppel HW, Kautz M, Xu C, et al. An overview: fatigue behaviour of ultrafine-grained metals and alloys. Int J Fatigue. 2006;28:1001–1010.

[68] Langdon TG. Seventy-five years of superplasticity: historic developments and new opportunities. J Mater Sci. 2009;44:5998–6010.

[69] Barnes AJ. Superplastic forming 40 years and still growing. J Mater Eng Perform. 2007;16:440–454.

[70] Langdon TG. A unified approach to grain-boundary sliding in creep and superplasticity. Acta Metall Mater. 1994;42:2437–2443.

[71] Valiev RZ, Salimonenko DA, Tsenev NK, Berbon PB, Langdon TG. Observations of high strain rate superplasticity in commercial aluminum alloys with ultrafine grain sizes. Scripta Mater. 1997;37:1945–1950.

[72] Horita Z, Furukawa M, Nemoto M, Barnes AJ, Langdon TG. Superplastic forming at high strain rates after severe plastic deformation. Acta Mater. 2000;48: 3633–3640.

[73] Akamatsu H, Fujinami T, Horita Z, Langdon TG. Influence of rolling on the superplastic behavior of an Al-Mg-Sc alloy after ECAP. Scripta Mater. 2001;44:759–764.

[74] Horita Z, Matsubara K, Makii K, Langdon TG. A two-step processing route for achieving a superplastic forming capability in dilute magnesium alloys. Scripta Mater. 2002;47:255–260.

[75] Furui M, Kitamura H, Anada H, Langdon TG. Influence of preliminary extrusion conditions on the superplastic properties of a magnesium alloy processed by ECAP. Acta Mater. 2007;55:1083–1091.

[76] Figueiredo RB, Langdon TG. Record superplastic ductility in a magnesium alloy processed by equal-channel angular pressing. Adv Eng Mater. 2008;10: 37–40.

[77] Avtokratova E, Sitdikov O, Markushev M, Mulyukov R. Extraordinary high-strain rate superplasticity of severely deformed Al-Mg-Sc-Zr alloy. Mater Sci Eng A. 2012;538:386–390.

[78] Kawasaki M, Langdon TG. Developing superplasticity and a deformation mechanism map for the Zn-Al eutectoid alloy processed by high-pressure torsion. Mater Sci Eng A. 2011;528:6140–6145.

[79] Han SZ, Lim C, Kim C, Kim S. The microstructural evolution during the equal channel angular pressing process and its relationship with the tensile behavior of oxygen-free copper. Metall Mater Trans A. 2005;36A: 467–470.

[80] Habibi A, Ketabchi M, Eskandarzadeh M. Nano-grained pure copper with high-strength and high-conductivity produced by equal channel angular rolling process. J Mater Processing Technol. 2011;211:1085–1090.

[81] Higuera OF, Munoz JA, Cabrera JM. Mechanical properties of different coppers processed by equal channel angular pressing. Mater Sci Forum. 2011;667–669:713–718.

Downloaded by [University of Southampton] at 06:30 17 February 2016

[82] Edalati K, Imamura K, Kiss T, Horita Z. Equal-Channel angular pressing and high-pressure torsion of pure copper: evolution of electrical conductivity and hardness with strain. Mater Trans. 2012;53:123–127.

[83] Jang Y, Kim S, Han S, Lim C, Kim C, Goto M. Role of trace elements on tensile behavior of accumulative roll-bonded pure copper. J Mater Sci. 2005;40:3527–3529.

[84] Hosseini SA, Manesh HD. High-strength, high-conducti vity ultra-fine grains commercial pure copper produced by ARB process. Mater Des. 2009;30:2911–2918.

[85] Takata N, Lee SH, Tsuji N. Ultrafine grained copper alloy sheets having both high strength and high electric conductivity. Mater Lett. 2009;63:1757–1760.

[86] Lee S, Matsunaga H, Sauvage X, Horita Z. Strengthening of Cu-Ni-Si alloy using high-pressure torsion and aging. Mater Characterization. 2014;90:62–70.

[87] Shangina DV, Gubicza J, Dodony E, et al. Improvement of strength and conductivity in Cu-alloys with the application of high pressure torsion and subsequent heat-treatments. J Mater Sci. 2014;49:6674–6681.

[88] Bobruk EV, Murashkin MY, Kazykhanov VU, Valiev RZ. Aging behavior and properties of ultrafine-grained aluminum alloys of Al-Mg-Si system. Rev Adv Mater Sci. 2012;31:109–115.

[89] Murashkin MY, Sabirov I, Kazykhanov VU, Bobruk EV, Dubravina AA, Valiev RZ. Enhanced mechanical properties and electrical conductivity in ultrafine-grained Al alloy processed via ECAP-PC. J Mater Sci. 2013;48:4501–4509.

[90] Valiev RZ, Murashkin MY, Sabirov I. A nanostructural design to produce high-strength Al alloys with enhanced electrical conductivity. Scripta Mater. 2014;76:13–16.

[91] Cubero-Sesin JM, In H, Arita M, Iwaoka H, Horita Z. High-pressure torsion for fabrication of high-strength and high-electrical conductivity Al micro-wires. J Mater Sci. 2014;49:6550–6557.

[92] Cubero-Sesin JM, Arita M, Watanabe M, Horita Z. High strength and high electrical conductivity of UFG Al-2% Fe alloy achieved by high-pressure torsion and aging. IOP Conf Series: Mater Sci Eng. 2014;63:012117.

[93] Berkowitz AE, Mitchell JR, Carey MJ, et al. Giant magnetoresistance in heterogeneous Cu-Co alloys. Phys Rev Lett. 1992;68:3745–3748.

[94] Xiao JQ, Jiang JS, Chien CL. Giant magnetoresistance in nonmultilayer magnetic systems. Phys Rev Lett. 1992;68:3749–3752.

[95] Takanashi K, Park J, Sugawara T, et al. Giant magnetoresistance and microstructure in Cr-Fe and Cu-Co heterogeneous alloys. Thin Solid Films. 1996;275:106–110.

[96] Wang WD, Zhu FW, Weng J, Xiao JM, Lai WY. Nanoparticle morphology in a granular Cu-Co alloy with giant magnetoresistance. Appl Phys Lett. 1998;72:1118–1120.

[97] Kim IJ, Takeda H, Echigoya J, Kataoka N, Fukamichi K, Shimada Y. The effect of aging on GMR and microstructure of Co10Cu90 ribbons. Mater Sci Eng A. 1996;217–218:363–366.

[98] Aizawa T, Zhou C. Nanogranulation process into magneto-resistant Co-Cu alloy on the route of bulk mechanical alloying. Mater Sci Eng A. 2000;285:1–7.

[99] Larde R, Le Breton JM. Influence of the milling conditions on the magnetoresistive properties of a Cu-80(Fe0.7Co0.3)(20) granular alloy elaborated by mechanical alloying. J Magnetism and Magnetic Mater. 2005;290–291:1120–1122.

[100] Rattanasakulthong W, Sirisathitkul C. Large negative magnetoresistance in capsulated Co-Cu powder prepared by mechanical alloying. Physica B. 2005;369:160–167.

[101] Massalski TB, Murray JL, Bennett LH, Baker H, Kacprzak L. Binary phase diagrams. Metals Park, OH: American Society of Metals; 1987.

[102] Suehiro K, Nishimura S, Horita Z, Mitani S, Takanashi K, Fujimori H. High-pressure torsion for production of magnetoresistance in Cu-Co alloy. J Mater Sci. 2008;43:7349–7353.

[103] Nishihata S, Suehiro K, Arita M, Masuda M, Horita Z. High-pressure torsion for giant magnetoresistance and better magnetic properties. Adv Eng Mater. 2010;12:793–797.

[104] Skripnyuk VM, Rabkin E, Estrin Y, Lapovok R. The effect of ball milling and equal channel angular pressing on the hydrogen absorption/desorption properties of Mg-4.95 wt% Zn-0.71 wt% Zr (ZK60) alloy. Acta Mater. 2004;52:405–414.

[105] Krystian M, Zehetbauer MJ, Kropik H, Mingler B, Krexner G. Hydrogen storage properties of bulk nanostructured ZK60 Mg alloy processed by equal channel angular pressing. J Alloys Compd. 2011;509S: 449–455.

[106] Jorge AM, Prokofiev E, de Lima GF, et al. An investigation of hydrogen storage in a magnesium-based alloy processed by equal-channel angular pressing. Int J Hydrogen Energy. 2013;38:8306–8312.

[107] Dornheim M. Thermodynamics of metal hydrides: tailoring reaction enthalpies of hydrogen storage materials. In: Moreno-Pirajan JC, editor. Thermodyna mics—interaction studies—-solids, liquids and gases. Rijeka: InTech; 2011. p. 891–918.

[108] Grill A, Horky J, Krexner G, Zehetbauer M. Long-term hydrogen storage Mg and ZK 60 after severe plastic deformation. Int J Hydr Energy. Forthcoming 2015.

[109] Botta WJ, Floriano R, Ishikawa TT, et al. Ultrafine grained Mg and Mg alloys for hydrogen storage. NANO2014. Moscow: Lomonosov Moscow State University; 2014. unpublished.

[110] Huot J, Skryabina NY, Fruchart D. Application of severe plastic deformation techniques to magnesium for enhanced hydrogen sorption properties. Metals. 2012;2:329–343.

[111] Leiva DR, Floriano R, Huot J, et al. Nanostructured MgH2 prepared by cold rolling and cold forging. J Alloys Compd. 2011;509S:444–448.

[112] Schober T, Westlake DG. The activation of FeTi for hydrogen storage—A different view. Scripta Metall. 1981;15:913–918.

[113] Mizuno T, Morozumi T. Titanium concentration in FeTiX (1 Less-Than-or-Equal-to X Less-Than-or-Equal-to 2) alloys and its effect on hydrogen storage properties. J Less-Common Metals. 1982;84: 237–244.

[114] Kulshreshtha SK, Jayakumar OD, Bhatt KB. Hydriding characteristics of palladium and platinum alloyed FeTi. J Mater Sci. 1993;28:4229–4233.

[115] Kulshreshtha SK, Sasikala R, Suryanarayana P, Singh AJ, Iyer RM. Studies on hydrogen storage material FeTi—effect of Sn substitution. Mater Res Bulletin. 1988;23:333–340.

[116] Su LY, Liu FJ, Bao DY. An advanced TiFe series hydrogen storage material with high hydrogen capacity

Downloaded by [University of Southampton] at 06:30 17 February 2016

and easily activated properties. Int J Hydrogen Energ. 1990;15:259–262.
[117] Chung HS, Lee JY. Hydriding and dehydriding reaction-rate of FeTi intermetallic compound. Int J Hydrogen Energ. 1985;10:537–542.
[118] Zuchner H, Kirch G. Auger-Electron spectroscopy investigation of the activation of TiFe for hydrogen uptake. J Less-Common Met. 1984;99:143–150.
[119] Trudeau ML, Schulz R, Zaluski L, et al. Nanocrystalline iron-titanium alloys prepared by high-energy mechanical deformation. Mech Alloy. 1992;88:537–544.
[120] Zaluski L, Tessier P, Ryan DH, et al. Amorphous and nanocrystalline Fe-Ti prepared by Ball-Milling. J Mater Res. 1993;8:3059–3068.
[121] Edalati K, Matsuda J, Iwaoka H, Toh S, Akiba E, Horita Z. High-pressure torsion of TiFe intermetallics for activation of hydrogen storage at room temperature with heterogeneous nanostructure. Int J Hydrogen Energ. 2013;38:4622–4627.
[122] Edalati K, Matsuda J, Arita M, Daio T, Akiba E, Horita Z. Mechanism of activation of TiFe intermetallics for hydrogen storage by severe plastic deformation using high-pressure torsion. Appl Phys Lett. 2013;103:143902.
[123] Edalati K, Matsuda J, Yanagida A, Akiba E, Horita Z. Activation of TiFe for hydrogen storage by plastic deformation using groove rolling and high-pressure torsion: similarities and differences. Int J Hydrogen Energ. 2014;39:15589–15594.
[124] Mujica A, Rubio A, Munoz A, Needs RJ. High-pressure phases of group-IV, III-V, and II-VI compounds. Rev Mod Phys. 2003;75:863–912.
[125] Islamgaliev RK, Kuzel R, Mikov SN, et al. Structure of silicon processed by severe plastic deformation. Mater Sci Eng A. 1999;266:205–210.
[126] Ikoma Y, Hayano K, Edalati K, Saito K, Guo QX, Horita Z. Phase transformation and nanograin refinement of silicon by processing through high-pressure torsion. Appl Phys Lett. 2012;101:121908.
[127] Ikoma Y, Hayano K, Edalati K, et al. Fabrication of nanograined silicon by high-pressure torsion. J Mater Sci. 2014;49:6565–6569.
[128] Valiev RZ, Ivanisenko YV, Rauch EF, Baudelet B. Structure and deformation behaviour of armco iron subjected to severe plastic deformation. Acta Mater. 1996;44:4705–4712.
[129] Ito Y, Horita Z. Microstructural evolution in pure aluminum processed by high-pressure torsion. Mater Sci Eng A. 2009;503:32–36.
[130] Delley B, Steigmeier EF. Quantum confinement in Si nanocrystals. Phys Rev B. 1993;47:1397–1400.
[131] Islamgaliev RK, Kuzel R, Obraztsova ED, Burianek J, Chmelik F, Valiev RZ. TEM, XRD and Raman scattering of germanium processed by severe deformation. Mater Sci Eng A. 1998;249:152–157.
[132] Ikoma Y, Ejiri Y, Hayano K, Saito K, Guo QX, Horita Z. Nanograin formation of GaAs by high-pressure torsion. Philos Mag Lett. 2014;94:1–8.
[133] Pavesi L, Dal Negro L, Mazzoleni C, Franzo G, Priolo F. Optical gain in silicon nanocrystals. Nature. 2000;408:440–444.
[134] Cullis AG, Canham LT. Visible-light emission due to quantum size effects in highly porous crystalline silicon. Nature. 1991;353:335–338.
[135] Ruckschloss M, Landkammer B, Veprek S. Light-emitting nanocrystalline silicon prepared by dry processing—the effect of crystallite size. Appl Phys Lett. 1993;63:1474–1476.
[136] Croitoru MD, Shanenko AA, Peeters FM. Dependence of superconducting properties on the size and shape of a nanoscale superconductor: from nanowire to film. Phys Rev B. 2007;76:024511.
[137] Suematsu H, Kato M, Ishida T. Critical temperature in nanoscopic superconductors. 25th International Conference on Low Temperature Physics (LT25), PT 5a; 2009:150:052250.
[138] Schweigert VA, Peeters FM, Deo PS. Vortex phase diagram for mesoscopic superconducting disks. Phys Rev Lett. 1998;81:2783–2786.
[139] Guo Y, Zhang YF, Bao XY, et al. Superconductivity modulated by quantum size effects. Science. 2004;306:1915–1917.
[140] Savolainen M, Touboltsev V, Koppinen P, Riikonen KP, Arutyunov K. Ion beam sputtering for progressive reduction of nanostructures dimensions. Appl Phys A. 2004;79:1769–1773.
[141] Nishizaki T, Lee S, Horita Z, Sasaki T, Kobayashi N. Superconducting properties in bulk nanostructured niobium prepared by high-pressure torsion. Physica C. 2013;493:132–135.
[142] Lee S, Horita Z. High-pressure torsion for pure chromium and niobium. Mater Trans. 2012;53:38–45.
[143] Edalati K, Daio T, Lee S, et al. High strength and superconductivity in nanostructured niobium-titanium alloy by high-pressure torsion and annealing: significance of elemental decomposition and supersaturation. Acta Mater. 2014;80:149–158.
[144] Poole JCP, Farach HA, Creswick RJ, Prozorov R. Superconductivity. 2nd ed. Amsterdam: Elsevier; 2007.
[145] Rogl G, Rogl P, Bauer E, Zehetbauer M. Severe plastic deformation, A tool to enhance thermoelectric performance. In: Koumoto K, Mori T, editors. Thermoelectric nanomaterials. Berlin: Springer; 2013. p. 193–254.
[146] Dresselhaus MS, Heremans JP. Recent developments in low dimensional thermoelectric material. In: Rowe DM, editor. Thermoelectric handbook. Macro to nanostructured materials. Boca Raton, FL, USA: CRC Press; 2004. p. 39.1–39.20.
[147] Ashida M, Hamachiyo T, Hasezaki K, Matsunoshita H, Kai M, Horita Z. Texture of bismuth telluride-based thermoelectric semiconductors processed by high-pressure torsion. J Phys Chem Solid. 2009;70:1089–1092.
[148] Hayashi T, Horio Y, Takizawa H. Equal channel angular extrusion technique for controlling the texture of n-type Bi2Te3 based thermoelectric materials. Mater Trans. 2010;51:1914–1918.
[149] Zhang L, Grytsiv A, Bonarski B, et al. Impact of high pressure torsion on the microstructure and physical properties of Pr0.67Fe3CoSb12, Pr0.71Fe3.5Ni0.5Sb12, and Ba0.06Co4Sb12. J Alloys Compd. 2010;494:78–83.
[150] Rogl G, Grytsiv A, Rogl P, et al. Dependence of thermoelectric behaviour on severe plastic deformation parameters: a case study on p-type skutterudite DD0.60Fe3CoSb12. Acta Mater. 2013;61:6778–6789.
[151] Rogl G, Grytsiv A, Rogl P, et al. n-Type skutterudites (R,Ba,Yb)(y)Co4Sb12 (R = Sr, La, Mm, DD, SrMm, SrDD) approaching ZT approximate to 2.0. Acta Mater. 2014;63:30–43.

Downloaded by [University of Southampton] at 06:30 17 February 2016

[152] Rogl G, Grytsiv A, Heinrich P, et al. New p-type skutterudites DD0.7Fe2.7Co1.3Sb12-xXx (X = Ge, Sn) reaching ZT > 1.3. Acta Mater. 2015;91: 227–238.
[153] Rogl G, Grytsiv A, Bursik J, et al. Changes in microstructure and physical properties of skutterudites after severe plastic deformation. Phys Chem Chem Phys. 2015;17:3715–3722.
[154] Straumal BB, Gornakova AS, Mazilkin AA, et al. Phase transformations in the severely plastically deformed Zr-Nb alloys. Mater Lett. 2012;81:225–228.
[155] Lowe TC, Valiev RZ. Frontiers of bulk nanostructured metals in biomedical applications. In: Tiwari A, Nordin AN, editors. Advanced biomaterials and biodevices. Beverly, MA: Wiley-Scrivener; 2014. p. 3–52.
[156] Valiev RZ, Semenova IP, Latysh VV, Rack H, Lowe TC, Petruzelka J, Dluhos L, Hrusak D, Sochova J. Nanostructured titanium for biomedical applications. Adv Eng Mater. 2008;10:B15–B17.
[157] Park JW, Kim YJ, Park CH, Enhanced osteoblast response to an equal channel angular pressing-processed pure titanium substrate with microrough surface topography. Acta Biomater. 2009;5:3272–3280.
[158] Mishnaevsky L, Levashov E, Valiev RZ, et al. Nanostructured titanium-based materials for medical implants: modeling and development. Mater Sci Eng R. 2014;81: 1–19.
[159] Bagherifard S, Gheichi R, Khademhosseini A, Guagliano M. Cell response to nanocrystallized metallic substrates obtained through severe plastic deformation. ACS Appl Mater Interfaces. 2014;6: 7963–7985.
[160] Estrin Y, Kasper C, Diederichs S, Lapovok R. Accelerated growth of preosteoblastic cells on ultrafine grained titanium. J Biomed Mater Res Part A. 2009;90A:1239–1242.
[161] Estrin Y, Kim HE, Lapovok R, Ng HP, Jo JH. Mechanical strength and biocompatibility of ultrafine-grained commercial purity titanium. Biomed Res Int. 2013;2013:6, Article ID 914764. doi:10.1155/2013/914764.
[162] Niinomi M. Mechanical biocompatibilities of titanium alloys for biomedical applications. J Mech Behav Biomed Mater. 2008;1:30–42.
[163] Furuta T, Hara M, Horita Z, Kuramoto S. Severe plastic deformation in gum metal with composition at the structural stability limit. Int J Mater Res. 2009;100: 1217–1221.
[164] Yilmazer H, Niinomi M, Nakai M, et al. Mechanical properties of a medical beta-type titanium alloy with specific microstructural evolution through high-pressure torsion. Mater Sci Eng C. 2013;33:2499–2507.
[165] Sulkowski B, Panigrahi A, Ozaltin K, Lewandowska M, Mikulowski B, Zehetbauer M. Evolution of strength and structure during SPD processing of Ti-45Nb alloys: experiments and simulations. J Mater Sci. 2014;49: 6648–6655.
[166] Panigrahi A, Bönisch M, Waitz T, et al. Phase transformations and mechanical properties of biocompatible Ti-16.1Nb processed by severe plastic deformation. J Alloys Compd. 2015;628:434–441.
[167] Matsumoto H, Watanabe S, Hanada S. Microstructures and mechanical properties of metastable beta TiNbSn alloys cold rolled and heat treated. J Alloys Compd. 2007;439:146–155.
[168] Panigrahi A, Sulkowski B, Waitz T, et al. Mechanical properties and texture evolution in biocompatible Ti-45Nb alloy processed by severe plastic deformation. J Mech Beh Biomed Mater. 2015; submitted.
[169] Brar HS, Platt MO, Sarntinoranont M, Martin PI, Manuel MV. Magnesium as a biodegradable and bioabsorbable material for medical implants. J Mater. 2009;61:31–34.
[170] Waizy H, Seitz JM, Reifenrath J, et al. Biodegradable magnesium implants for orthopedic applications. J Mater Sci. 2013;48:39–50.
[171] Kubasek J, Vojtech D, Capek J. Properties of biodegradable alloys usable for medical purposes. Acta Physica Polonica A. 2012;122:520–523.
[172] Weber J. United States patent No. 8,435,281 B2. 2013.
[173] Yamashita A, Horita Z, Langdon TG. Improving the mechanical properties of magnesium and a magnesium alloy through severe plastic deformation. Mater Sci Eng A. 2001;300:142–147.
[174] Agnew SR, Stoica GM, Chen LJ, Lillo TM, Macheret J, Liaw PK. Equal channel angular processing of magnesium alloys. In: Zhu YT, Langson TG, et al., editors. Ultrafine Grained Mater II, TMS Meeting. TMS Publications, USA; 2002.
[175] Kainer KU, Huang Y, Peng Q, Hort N. Nanostructured magnesium alloys. Nanostructured metals: Fundementals to applications. Riso International Symposium on Meterial Science. Roskilde: Denmark Tekniske Universitet, Riso Nationallaboratoriet for Baeredygtig Energi. Proceedings 2009;30:81–99.
[176] Guo W, Wang QD, Ye B, Zhou H. Microstructure and mechanical properties of AZ31 magnesium alloy processed by cyclic closed-die forging. J Alloys Compd. 2013;558:164–171.
[177] Shumilin SE, Janecek M, Isaev NV, Minarik P, Kral R. Low temperature plasticity of ultrafine-grained AE42 and AZ31 magnesium alloys. Adv Eng Mater. 2013;15: 352–357.
[178] Wang H, Estrin Y, Fu H, Song G, Zuberova Z. The effect of pre-processing and grain structure on the biocorrosion and fatigue resistance of magnesium alloy AZ31. Adv Eng Mater. 2007;9:967–972.
[179] Hadzima B, Janecek M, Suchy P, Mueller J, Wagner L. Microstructure and corrosion properties of fine-grained Mg-based alloys. Mater Sci Forum. 2008;584–586: 994–999.
[180] Minarik P, Kral R, Janecek M. Effect of ECAP processing on corrosion resistance of AE21 and AE42 magnesium alloys. Appl Surf Sci. 2013;281: 44–48.
[181] Hofstetter J, Becker M, Martinelli E, et al. High-strength low-alloy (HSLA) Mg-Zn-Ca alloys with excellent biodegradation performance. J Mater. 2014;66: 566–572.
[182] Hofstetter J, Martinelli E, Weinberg AM, et al. Assessing the degradation performance of ultrahigh-purity magnesium in vitro and in vivo. Corros Sci. 2015;91: 29–36.
[183] Horky J, Ghaffar A, Grill A, et al. Mechanical properties and microstructure of HPT-processed Mg-Zn-Ca alloys for biodegradable implants. In: Beausir B, Kasprzak N, Toth LS, editors. 6th international conference on nanomaterials by severe plastic deformation (NANOSPD6). Metz: University Press of Lorrain University; 2014.

[184] Zehetbauer M. Effects of nonequilibrium vacancies on strengthening. Key Eng Mater. 1994;97–98: 287–306.
[185] Zehetbauer MJ, Steiner G, Schafler E, Korznikov A, Korznikova E. Deformation induced vacancies with severe plastic deformation: measurements and modelling. Mater Sci Forum. 2006;503–504:57–64.
[186] Hampshire JM, Hardie D. Hardening of pure magnesium by lattice-defects. Acta Metallurgica. 1974;22: 657–663.
[187] Valiev RZ. Nanostructuring of metals by severe plastic deformation for advanced properties. Nature Mater. 2004;3:511–516.
[188] Ivanisenko Y, Darbandi A, Dasgupta S, Kruk R, Hahn H. Bulk nanostructured materials: non-mechanical synthesis. Adv Eng Mater. 2010;12:666–676.
[189] Valiev RZ, Langdon TG. The art and science of tailoring materials by nanostructuring for advanced properties using SPD techniques. Adv Eng Mater. 2010;12: 677–691.

Downloaded by [University of Southampton] at 06:30 17 February 2016